European Journal of Medicinal Chemistry 144 (2018) 262–276

Contents lists available at ScienceDirect

European Journal of Medicinal Chemistry

journal homepage: http://www.elsevier.com/locate/ejmech

Research paper

1,3,5-triazaspiro[5.5]undeca-2,4-dienes as selective *Mycobacterium tuberculosis* dihydrofolate reductase inhibitors with potent whole cell activity

Xuan Yang [a, 1], Wassihun Wedajo [b, 1], Yoshiyuki Yamada [b], Sue-Li Dahlroth [c], Jason Jun-Long Neo [c], Thomas Dick [b, d, *], Wai-Keung Chui [a, **]

[a] Department of Pharmacy, Faculty of Science, National University of Singapore, 18 Science Drive 4, 117543, Singapore
[b] Department of Microbiology and Immunology, Yong Loo Lin School of Medicine, National University of Singapore, 5 Science Drive 2, 117545, Singapore
[c] Protein Production Platform, School of Biological Sciences, Nanyang Technological University, 138673, Singapore
[d] Public Health Research Institute, New Jersey Medical School, Rutgers University, 225 Warren Street, Newark, NJ07103, USA

ARTICLE INFO

Article history:
Received 29 September 2017
Received in revised form
17 November 2017
Accepted 5 December 2017
Available online 7 December 2017

Keywords:
Dihydrofolate reductase (DHFR)
Antimycobacterial agent
Tuberculosis (TB)
1,3,5-triazaspiro[5.5]undeca-2,4-diene

ABSTRACT

The emergence of multi- and extensively-drug resistant tubercular (MDR- and XDR-TB) strains of mycobacteria has limited the use of existing therapies, therefore new drugs are needed. Dihydrofolate reductase (DHFR) has recently attracted much attention as a target for the development of anti-TB agents. This study aimed to develop selective *M. tuberculosis* DHFR inhibitors using rationale scaffolding design and synthesis, phenotype-oriented screening, enzymatic inhibitory study, whole cell on-target validation, molecular modeling, and *in vitro* DMPK determination to derive new anti-TB agents. 2,4-diamino-1-phenyl-1,3,5-triazaspiro[5.5]undeca-2,4-dienes **20b** and **20c** were identified as selective *M. tuberculosis* DHFR inhibitors, showing promising antimycobacterial activities (MIC_{50}: 0.01 μM and MIC_{90}: 0.025 μM on *M. tuberculosis* H37Rv). This study provided compelling evidence that compound **20b** and **20c** exerted whole cell antimycobacterial activity through DHFR inhibition. In addition, these two compounds exhibited low cytotoxicity and low hemolytic activity. The *in vitro* DMPK and physiochemical properties suggested their potential *in vivo* efficacy.

1. Introduction

Tuberculosis (TB) is one of the leading causes of death worldwide and this has become a global public health issue. In 2015, WHO estimated 10.4 million cases of new TB infections and reported that 1.8 million deaths were TB related [1]. The statistics from recent reports have shown that the prevalence of TB has escalated to an epidemic proportion. The emergence of multi and extensively drug-resistant TB (MDR-TB and XDR-TB) strains of *Mycobacterium tuberculosis* has limited the use of existing therapies, thus exacerbating the epidemic further. In 2015, the mortality cases due to MDR-TB were estimated at 0.25 million while among the people who were diagnosed with MDR-TB, an estimated 9.5% of them were suffering from XDR-TB [2]. In addition, within the HIV positive population of patients, opportunistic infection due to TB is contributing to increasing morbidity and mortality [3]. The epidemiology of the disease has raised deep concerns among clinicians and scientists therefore active efforts are underway to address this public health related issue.

The current treatment regimen for drug-sensitive TB consists of a combination of four first-line drugs namely, isoniazid, pyrazinamide, rifampicin and ethambutol [4]. The patients are required to adhere to the combination therapy for at least 6 months. In case of drug-resistant strains, the treatment period can

Abbreviations: DHFR, dihydrofolate reductase; DMPK, drug metabolism and pharmacokinetics; FRLM, female rat liver microsomes; HBA, hydrogen bond acceptors; HBD, hydrogen bond donors; MDR, multi-drug resistant; MRLM, male rat liver microsomes; *Mtb*, *M. tuberculosis*; MTX, methotrexate; NMR, nuclear magnetic resonance; SI, selectivity index; TB, tuberculosis; TPSA, topological polar surface area; XDR, extensively-drug resistant.

* Corresponding author. Department of Microbiology and Immunology, Yong Loo Lin School of Medicine, National University of Singapore, 5 Science Drive 2, 117545, Singapore.
** Corresponding author. Department of Pharmacy, Faculty of Science, National University of Singapore, 18 Science Drive 4, 117543, Singapore.
E-mail addresses: td367@njms.rutgers.edu (T. Dick), phacwk@nus.edu.sg (W.-K. Chui).

[1] These authors contribute equally to this work.

https://doi.org/10.1016/j.ejmech.2017.12.017
0223-5234/

be extended to 18–24 months with the inclusion of some second-line drugs such as fluoroquinolones, streptomycin, linezolid, *para*-aminosalicylic acid and others [5]. Apart from the high pill burden and the lengthy treatment, the therapies for TB can also be costly. Many second-line drugs are known to be toxic and less efficient, posing a significant barrier to patient compliance [6]. Hence, more efforts are needed to broaden the availability of treatment options by designing and synthesizing new anti-TB agents that exert different mechanism of action to circumvent the current drug resistance issue.

Dihydrofolate reductase (DHFR), a key enzyme in the folate pathway, is responsible for reducing dihydrofolic acid to tetrahydrofolic acid. Tetrahydrofolate is involved in one carbon transfer reactions that lead to the biosynthesis of nucleic acids and amino acids. Thus, the inhibition of DHFR is able to arrest cell growth by depleting the cellular pool of DNA, RNA and protein synthesis precursors [7,8]. DHFR has been recognized as a validated drug target for antibacterial agents [9]. However, few potent and selective DHFR inhibitors have so far been reported that exhibits anti-mycobacterial activity despite on-going research work in the scientific community [10]. For example, by using a well-known DHFR inhibitor, methotrexate (**MTX**) as lead compound, two esters of methotrexate (**JSF-1187** and **JSF-1183**) have been reported to demonstrate potent pathogenic DHFR inhibition activity (Fig. 1) by Nixon et al. [11]. Nevertheless, these two compounds have not shown significant selectivity for *M. tuberculosis* DHFR (*Mtb* DHFR) due to their close similarity with **MTX**. Besides the pteridine scaffold, three hits (**PDP-1**, **PQD-1** and **Dpt-1**, Fig. 1) representing other chemical scaffolds were identified by Kumar et al. through a phenotypic screening against live H37Rv strain of *Mtb*, and DHFR inhibitory activity evaluation [12]. However, only **Dpt-1** exhibited selectivity against pathogenic DHFR. Recently, Nilesh and colleagues have developed two 2,4-diamino-1,3,5-triazine derivatives (Fig. 1) that showed selective *Mtb* DHFR inhibition, and these two compounds were found to possess promising antitubercular activity and lower cytotoxicity in human [13]. Collectively, these reports suggested that there is potential pharmacotherapeutic significance in using DHFR inhibitors for the treatment of tuberculosis. The core structural feature for the inhibition of DHFR is known to be a diamino-substituted N-containing single or fused polycyclic heterocycle such as pyrimidine, quinazoline or pteridine. Many of these scaffolds have been extensively studied and demonstrated to possess antibacterial activity against various microorganisms [7,14,15]. Nonetheless, few studies were carried out on diamino-substituted N-containing spiro scaffold [16].

Over the years, in the main author's laboratory, the spiro heterocycle 1,3,5-triazaspiro[5.5]undeca-2,4-diene has demonstrated behaviours that can be exploited for selective DHFR inhibitory activity against pathogenic bacteria. For instance, **7s** (Fig. 2) was demonstrated to inhibit the growth of *Mycobacterium smegmatis* [16], while **P-I-23** (Fig. 2) was found to have no inhibitory action on recombinant human DHFR, and was also found to be non-toxic to A549 cell line human lung carcinoma [17]. Taken together, it was hypothesized that with appropriate substitution on the saturated nitrogen of this spiro heterocycle, selective mycobacterial DHFR inhibitor with low human cytotoxicity could be developed. The saturated nitrogen was selected as a point for side chain extension because it was believed that the side chain would be accommodated in a channel at the active site [13,18,19]. This paper reports a study that entailed the synthesis of new compounds having extension made to the saturated nitrogen (N1) of the 1,3,5-triazaspiro[5.5]undeca-2,4-diene by inserting either a methylene or a phenyl attachment. The side chain was elongated using click chemistry. This conjunctive approach was applied to search for new compounds with DHFR inhibitory activity. It is also reported that in the distal end of the side chain, there are amino acid residues that may offer hydrophobic and hydrogen-bonding interactions [18]. It was therefore proposed to have phenyl alkyl group, benzoyl methyl group, and coumarin alkyl group inserted into the distal end in an attempt to interact with this part of the enzyme (Fig. 2).

2. Results and discussion

2.1. Chemistry

All the compounds were designed and synthesized using strategies that extended the side chain at position N1 of the spiro heterocycle (Fig. 2). Based on compound **7s**, one strategy was to link N1 of 1,3,5-triazaspiro[5.5]undeca-2,4-diene and the 1,2,3-triazole with a methylene group to evaluate if a rotatable alkyl linker would be favour DHFR inhibition that might lead to anti-mycobacterial activity. This strategy resulted in the design of compounds **7a-7c**, **11a-11c** and **14** (Scheme 1). The second strategy was derived from compound **P-I-23** by attaching 4-methyleneoxy phenyl ring at N1 of 1,3,5-triazaspiro[5.5]undeca-2,4-diene and linking it to the triazole ring. This strategy afforded compounds **19a-19c**, **20a-20c** and **21** (Scheme 2A, 2B and 2C). In these two strategies, the three-component one-pot synthesis described by Modest's was used to generate the alkyne intermediates **4** and **18** as hydrochloric salt [20]. The intermediates were reacted with selected azido derivatives to give the target compounds.

2.1.1. Synthesis of target compounds *7a-7c, 11a-11c and 14*

As shown in Scheme 1, the modified three-component one pot synthetic strategy was adopted to generate intermediate **4** by refluxing propargylamine hydrochloride **1**, cyanoguanidine **2**, and cyclohexanone **3** in the presence of catalytic amount (0.2 equivalent) of concentrated hydrochloric acid in ethanol [20]. In the following step, the transformation of benzylbromides **5a-5c** into the corresponding azides **6a-6c** was achieved via a nucleophilic substitution of the bromide with three equivalents of sodium azide under reflux condition. The azide intermediate was used in the next step without further purification. The freshly prepared azides **6a-6c** were coupled to intermediate **4** via a 1,3-dipolar addition reaction in the presence of catalytic amount (0.1 equivalent) of copper sulfate. The reaction of intermediate **4** and azide **6a-6c** was monitored by TLC (MeOH: DCM = 1: 9) using UV as detector. The target products **7a-7c** were formed in reasonably good yield (61–68%) when the reflux was conducted in a solvent system of THF and water at volume ratio of 1:1. For the synthesis of compounds **9a-9c**, the ethereal spacer was furnished via Williamson synthesis by refluxing the corresponding dibromoalkanes and compound **8** in acetonitrile under basic condition. Potassium carbonate was used to deprotonate the phenolic group on umbelliferon **8**. Azide derivatives **10a-10c** were formed when compounds **9a-9c** were treated with sodium azide under reflux. The coupling reaction of the azide derivatives **10a-10c** and intermediate **4** produced the desired target products **11a-11c**. The synthesis of product **14** was similar to the preparation of products **7** and **11**. The acetophenone **12** was treated with sodium azide to afford the corresponding azide **13**, which was followed by coupling with intermediate **4** to furnish the desired target product **14**. The yield for the final-step reaction was further improved by dissolving the azide derivative in tetrahydrofuran and followed by dropwise addition of this azide solution into the reaction mixture with constant stirring.

2.1.2. Synthesis of target compounds *19a-19c, 20a-20c, and 21*

The synthetic schemes for compounds **19a-19c**, **20a-20c** and **21** are illustrated in Scheme 2A, 2B and 2C respectively. Prop-2-ynyloxy aniline **17** was prepared by a two-step reaction. Firstly, 4-

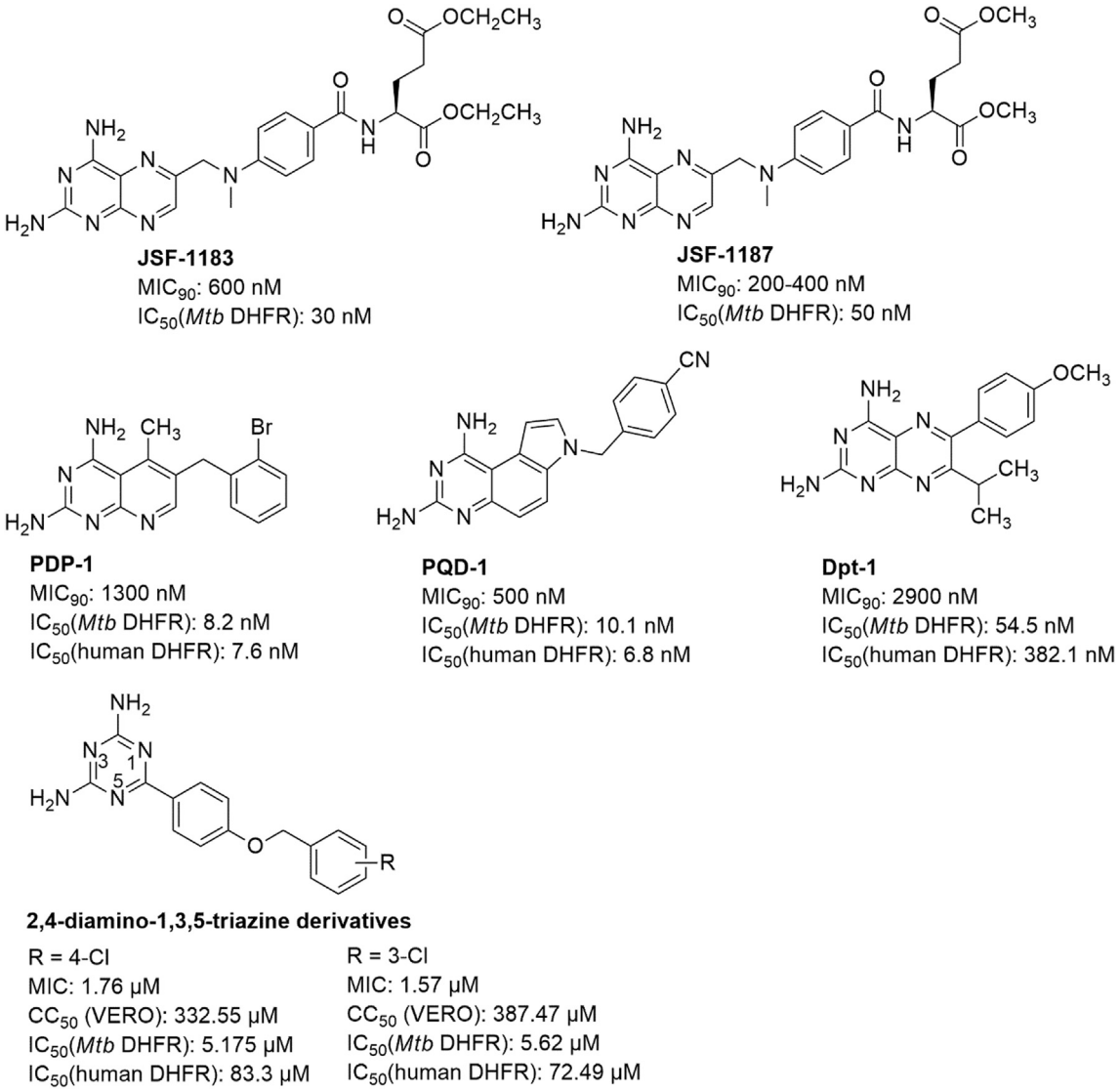

Fig. 1. The structures of reported *Mtb* DHFR inhibitors that exhibit antimycobacterial activity [10–12].

nitrophenol **15** was refluxed with propargyl bromide under basic condition to furnish 4-nitrophenyl-2-propynyl ether **16** via Williamson synthesis. The crude product was separated by filtering out the reaction mixture, and purified by column chromatography using ethyl acetate/hexane (1:5 to 1:1, v/v) as the mobile phase. Then the purified 4-nitrophenyl-2-propynyl ether **16** was reduced to 4-(prop-2-ynyloxy)aniline **17** by an excess of iron powder under acidic environment in excellent yields and purity. The crude product **17** was used directly in the next step without further purification. The synthesis of intermediate **18** was conducted through an "one-pot three components" synthesis employing 4-(prop-2-ynyloxy)aniline **17**, cyanoguanidine and cyclohexanone. This reaction consisted of a trimerization between nitrile and cyanide groups to provide biguanide *in situ*. The formation of the spiro ring was achieved through the condensation reaction between the biguanide intermediate and a cyclic ketone. Intermediate **18** was purified by recrystallization from 95% ethanol in moderate yield. By applying click chemistry, intermediate **18a** was coupled with the corresponding azido derivatives **6a-6c**, **10a-10c** and **13** separately to afford the desired target products **19a-19c**, **20a-20c** and **21**, respectively.

All the final products were characterized and confirmed by NMR and MS. The purity of the target compounds was determined by HPLC analysis, and all the products showed purity of 95% or above.

2.2. Phenotype-oriented screening and cytotoxicity study

Recent works from literature have highlighted the higher success of phenotypic whole cell screening for identifying first-in-class antibacterial agents when compared to biochemical target-based approaches [21]. Therefore, a phenotype-oriented screening strategy was adopted to evaluate antimycobacterial activity of the synthesized compounds, followed by cytotoxicity detemination.

2.2.1. Antimycobacterial activity against M. bovis BCG

For a preliminary antimycobacterial study, single point screening was conducted against *M. bovis* BCG at 25 μM. *M. bovis* BCG is widely used as an *in vitro* screening model for antitubercular drug discovery as the strain represents a non-pathogenic close relative to *M. tuberculosis* [22]. As shown in Table 1, compounds **19a-19c**, **20a-20c**, and **21** exhibited stronger inhibition in comparison to compounds **7a-7c**, **11a-11c**, and **14**. It was found that

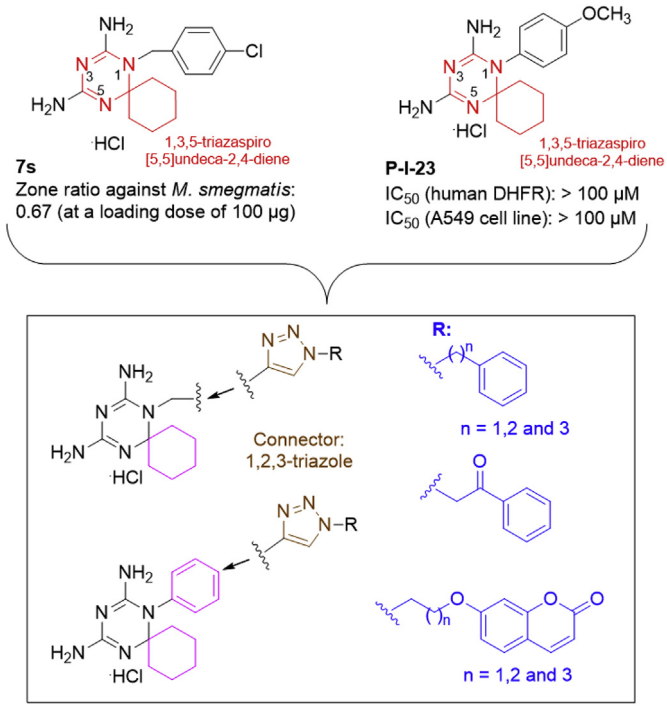

Fig. 2. Design of compounds by side chain extension at the saturated nitrogen of 1,3,5-triazaspiro[5.5]undeca-2,4-diene and 6,8,10-triazaspiro[4.5]deca-7,9-diene via click chemistry.

compounds having the 4-methyleneoxy phenyl linker at N1 of 1,3,5-triazaspiro[5.5]undeca-2,4-diene exhibited relatively higher antimycobacterial activity at 25 μM. Compounds that demonstrated at least 60% inhibition were selected for MIC_{50} value determination. The five selected compounds namely **19a**, **19c**, **20a**, **20b**, and **20c** were tested against *M. bovis* BCG by the broth microdilution method as described previously [23–25]. As shown in Table 1, compounds **20a**, **20b**, and **20c** exhibited more potent antimycobacterial activity (MIC_{50}: 0.01–0.2 μM) against *M. bovis* BCG, as compared to compounds **19a** and **19c**. The potency of compounds **20a-20c** may be attributed to the incorporation of the coumarin fragment, which can form potential hydrogen bonds with amino acid residues at the distal binding site. In particular, compounds **20b** and **20c** demonstrated both MIC_{50} and MIC_{90} values at sub-micro molar ranges. Besides, it can be seen that the antimycobacterial activity increased with the elongation of ethereal linker from 2 to 4 methylene groups.

2.2.2. Antimycobacterial activity against M. tuberculosis and cytotoxicity evaluation

To confirm the inhibitory activity against pathogenic *M. tuberculosis*, the most promising compounds **20b** and **20c** were tested against *M. tuberculosis* H37Rv. Both compounds showed antitubercular activity at MIC_{50} value of 0.01 μM and MIC_{90} value of 0.025 μM (Table 2). The excellent antitubercular activity of the two compounds prompted the need to evaluate their cytotoxic and hemolysis effects, by using the HepG2 cell line and red blood cells for CC_{50} and LC_{50} determination, respectively. Both compounds demonstrated low liver cell cytotoxicity and low hemolytic activity up to 100 μM. Consequently, both compounds **20b** and **20c**, with over 4000-fold selectivity, were subjected to DHFR inhibition determination.

2.3. Evaluation of in vitro Mtb DHFR and human DHFR inhibitory activities of compounds 20b, 20c, 19c and 11c

The two most potent compounds **20b** and **20c** were tested for their ability to inhibit recombinant *Mtb* DHFR as well as the recombinant human (rh) DHFR in an attempt to investigate their selectivity for inter-species enzymatic inhibition. The selectivity index (**SI**) was calculated as a ratio of the IC_{50} values of rh DHFR to the IC_{50} values of *Mtb* DHFR. Methotrexate, a very potent non-selective DHFR inhibitor, was used as control. As shown in Table 3, the IC_{50} values of the two compounds **20b** and **20c** indicated that they were less potent than methotrexate in inhibiting rh DHFR. However, they were 44–93 times more selective for r*Mtb* DHFR than methotrexate. Besides, it was found that the selectivity increased with the elongation of the ethereal linker from 3 to 4 methylene groups.

In order to explore the role of coumarin in DHFR binding, compound **19c** was selected for the enzyme inhibition assays. Through the comparison with compound **20b**, it was found that the incorporation of coumarin at the distal side chain increased potency as well as selectivity. In addition, the attachment of 4-methyleneoxy phenyl linker at N1 of 1,3,5-triazaspiro[5.5]undeca-2,4-diene was found to be essential for recombinant *Mtb* DHFR inhibition as well, by testing compound **11c** on *Mtb* DHFR.

However, it was found that the enzymatic inhibitory activities were not as potent as the whole cell antimycobacterial activities. This could be for instance due to the influence of the inclusion of His-tag on the recombinant *Mtb* DHFR or to accumulation of the test compounds in the bacterial cell. To exclude the possibility that the compounds may exert their whole cell antibacterial growth inhibition activity off target, on-target verification was conducted.

2.4. On target activity verification through M. bovis BCG DHFR overexpression and observation of MIC shift

In order to determine whether whole cell antimycobacterial activity was mediated indeed through DHFR inhibition, growth inhibition dose response experiments were carried out with a BCG strain that overexpressed DHFR. To achieve the overexpression, the DHFR gene *dfrA* was expressed under the control of the strong constitutive hsp60 promoter [26]. 10-fold *dfrA* overexpression was confirmed at the mRNA level by qRT-PCR. *p*-Aminosalicylic acid (PAS), a second-line anti-TB drug, was recently reported to be a prodrug, which is metabolized by folate pathway and inhibits DHFR. Hence, PAS was used as a positive control in this study (Fig. 3B), and the MIC_{90} value was shifted by 16 fold to a higher value. In terms of compounds **20b** and **20c**, the growth inhibition curves illustrated in Fig. 3A, show an MIC_{90} shift to a higher value in the DHFR-overexpressed (DHFR-oe) strain. Both compounds **20b** and **20c** exhibited a 25–30 fold shift, respectively, in the MIC_{90} (DHFR-oe BCG MIC_{90}/wt-BCG MIC_{90}) to higher values in the DHFR-oe strain compared with wild type *M. bovis* BCG. Taken together, these results suggested that these compounds exert their whole cell antimycobacterial activity via the inhibition of DHFR.

2.5. In silico molecular modeling of compound 20c in Mtb and human DHFRs

To better understand the binding interactions at the active site of both *Mtb* DHFR and human DHFR, *in silico* molecular modeling was conducted on compound **20c** due to its on-target inhibitory activity and better selectivity for r*Mtb* DHFR. Crystal strcutures of *Mtb* DHFR (PDB ID: 1DF7) and human DHFR (PDB ID: 2w3m) were obtained from the protein data bank (PDB) and modified for the docking experiments. Subsequently, the partial atomic charge

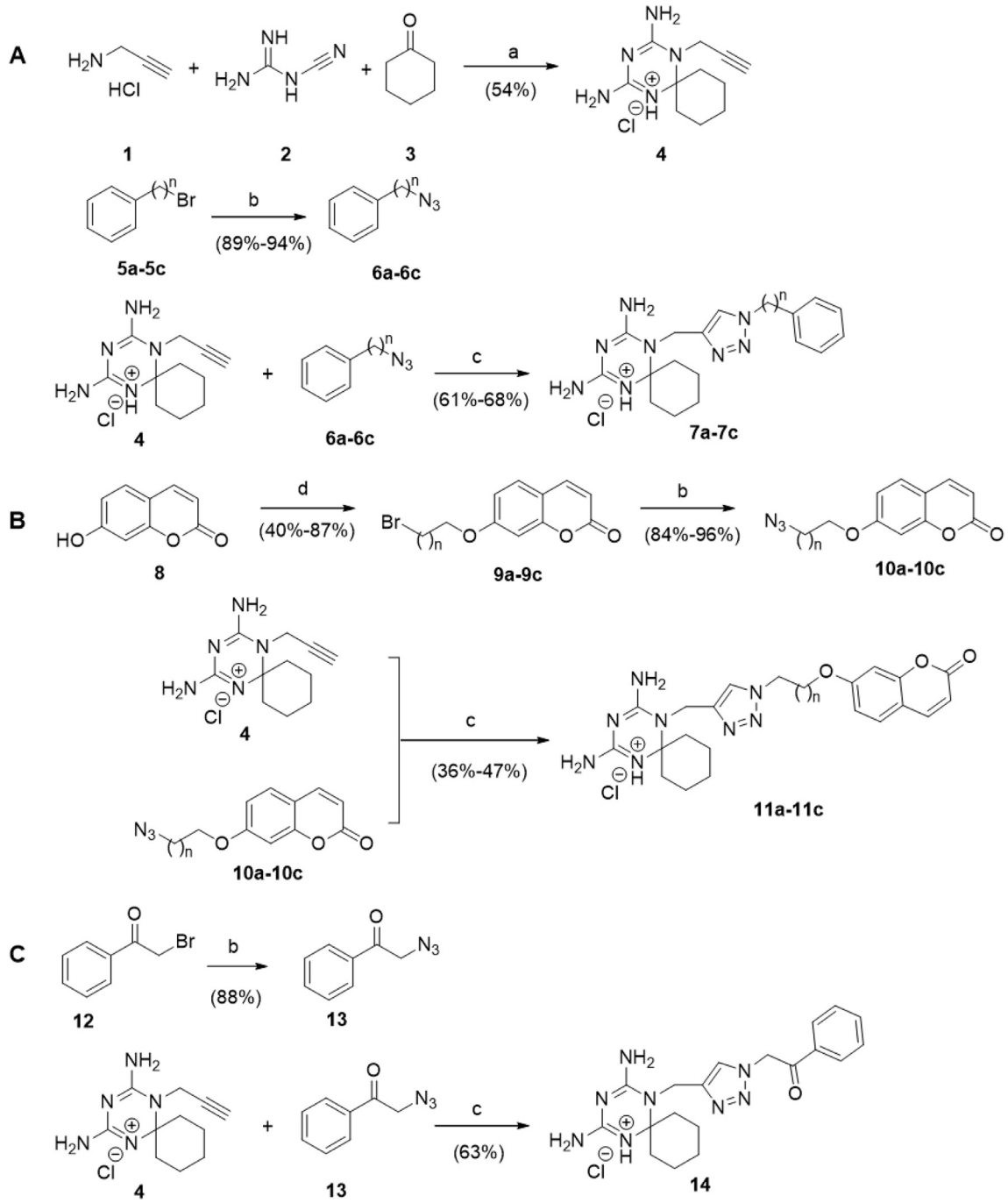

Scheme 1. Synthesis of triazaspiroalkenes **7a-7c** (**A**), **11a-11c** (**B**) and **14** (**C**). Reagents and conditions: (a) EtOH, Conc. HCl (0.2 equiv), reflux; (b) NaN_3 (3 equiv), DMF, reflux; (c) $CuSO_45H_2O$ (0.1 equiv), Sodium ascorbate (0.3 equiv), THF/H_2O (1:1, v/v), rt; (d) dibromoalkane, K_2CO_3 (6.0 equiv), acetonitrile, reflux.

distribution calculation and energy minimization of the ligands were performed before conducting the docking experiments. The docking protocol was optimized and validated by reproducing the observed co-crystallized ligands in *Mtb* DHFR (RMSD value of 1.06 Å) and human DHFR (RMSD value of 0.85 Å) respectively. The scoring function for docking is expressed as -log K_d which represents binding affinity in terms of hydrophobicity, polarity, repulsive forces, entropy, solvation and crash score. A higher docking score indicates tighter binding between the ligand and the receptor. The pose of compound **20c** with the highest docking score was selected, and its docking scores for both enzymes are summarized in Table 4. It was found that compound **20c** exhibited stronger binding affinity to *Mtb* DHFR as compared to its binding in human DHFR. This observation was consistent with the selectivity observed in the enzyme inhibition study.

As shown in Fig. 4A, compound **20c** binds in the active site of DHFR through the formation of hydrogen bonds with Ile94 (N-H···O: 1.84 Å), Ile5 (N-H···O: 1.82 Å), Tyr100 (N-H···O: 2.86 Å) and Asp 27 (N-H···O: 1.90 Å and 2.56 Å). Also, hydrogen bonds between 1,2,3-triazole and Leu24 (N-H···N: 2.19 Å), as well as between the oxygen from 1-(4-methoxy)phenyl ring and Trp22 (N-H···O: 2.52 Å) are also observed. Furthermore, another three favourable

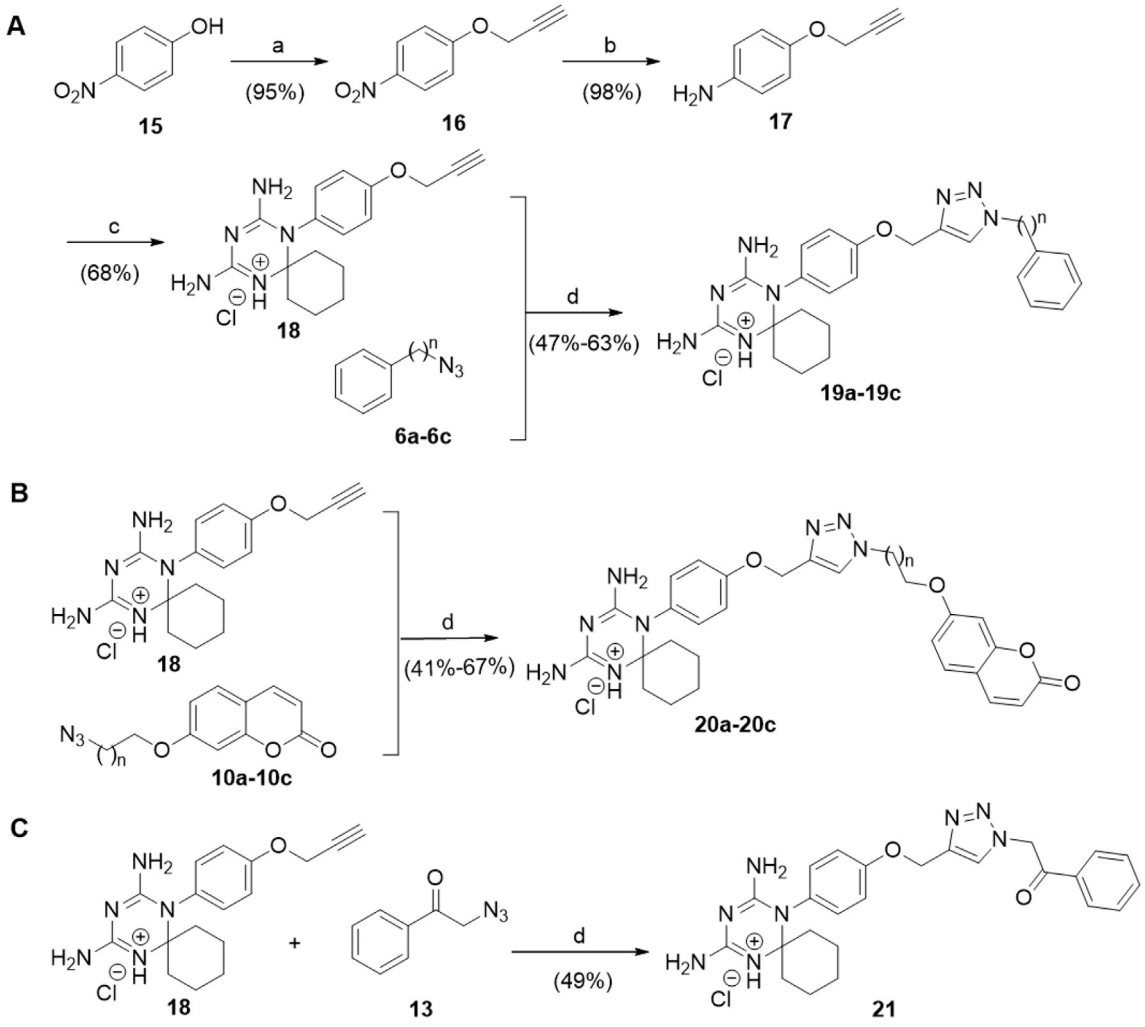

Scheme 2. (**A**) Synthesis of triazaspiroalkenes **19a-19c** (**A**), **20a-20c** (**B**), and **21** (**C**). Reagents and conditions: (a) propargyl bromide, K_2CO_3 (1.05 equiv.), acetonitrile, reflux; (b) Fe (6.5 equiv.), NH_4Cl (0.9 equiv), ethanol/water (5:1), reflux; (c) cyclohexanone, dicyandiamide, Conc. HCl (1.2 equiv.), EtOH, reflux; (d) $CuSO_45H_2O$ (0.1 equiv), Sodium ascorbate (0.3 equiv), THF/H_2O (1:1, v/v), rt.

hydrogen bonds were established between the distal ethereal oxygen and Gln28 (N-H···O: 2.85 Å), as well as between the carbonyl oxygen on coumarin and Arg32 (N-H···O: 2.19 Å), and Arg60 (N-H···O: 2.05 Å), respectively. In addition, hydrophobic amino residues Leu57, Val54, Pro51, Phe31, Leu24, and Ile20 make close contacts with the side chain (Fig. 4B). As a consequence, the insertion of 4-methyleneoxy phenyl linker between the DHFR pharmacophoric scaffold and 1,2,3-triazole has allowed conducive orientation of the DHFR pharmacophoric scaffold and 1,2,3-triazole side chain at the active site.

As compound **20c** demonstrated better inhibition activity for r*Mtb* DHFR over rh DHFR, the molecular modeling of compound **20c** in human DHFR was also conducted. As shown in Fig. 4C, the 2-amino group forms hydrogen bonds with Tyr121 (N-H···O: 2.62 Å) and Ile7 (N-H···O: 2.22 Å), while the 4-amino group forms hydrogen bond with Glu30 (N-H···O: 2.09 Å) at the DHFR anchoring point. Besides, a salt bridge (N-H···O: 2.06 Å) is established between protonated N5 of 1,3,5-triazine and carboxylate side chain of Glu30. Two additional hydrogen bonds are formed between the distal ethereal oxygen on coumarin and Arg70 (N-H···O: 2.10 Å), and between the lactone oxygen and Lys66 (N-H···O: 2.06 Å). Hydrophobic interactions (Fig. 4D) are involved with Trp24, Leu22, Phe31, Phe34, Val115, Leu67 and Ile60.

Through the comparison of the corresponding interactions at the different binding pockets, more favourable hydrogen bonding interactions were observed in *Mtb* DHFR active site by the incorporation of 1,2,3-triazole and the coumarin scaffold. In addition, as shown in Fig. 4D, though Phe31 and Leu22 could offer hydrophobic interaction with the cyclohexyl spiro ring, they might also restrict the entry of the inhibitor into the human DHFR anchoring point. In contrast, the entrance to *Mtb* DHFR anchoring pocket appeared wider and was able to accommodate the larger spiro ring. This observation was also supported by Elaine F and colleagues' finding that the distance between the side chains of Leu22 and Phe31 in human DHFR is at least 2-fold shorter than the distance between corresponding residues in *Mtb* DHFR [19]. It was also reported by Elaine F et al. that a water molecule interacted with Trp22, Asp27 and Gln28 that collectively formed a pocket in *Mtb* DHFR. In contrast, the corresponding binding pocket created by Leu20, Arg23, and Gln28 in human DHFR restricted the accessibility of methothrexate to the solvent. As shown in Fig. 4A, the 4-methyleneoxy phenyl linker of compound **20c** interacted with Trp22 via hydrogen bonding, while the coumarin scaffold formed hydrogen bonding with Gln28. Recent study highlighted the existence of glycerol binding site in the *Mtb* DHFR; however, the glycerol binding site is essentially absent in human DHFR [27]. Besides,

Table 1
Antimycobacterial activity of synthesized compounds against *M. bovis* BCG.

Cpd	Structure	Inhibition (%) at 25 μM	MIC_{50} (μM)	MIC_{90} (μM)
		M. bovis BCG	*M. bovis* BCG	*M. bovis* BCG
7a	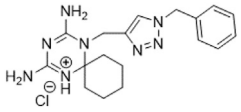	4.5	N.D	N.D
7b	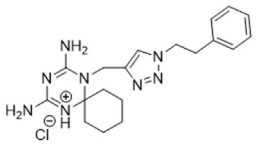	4.7	N.D	N.D
7c	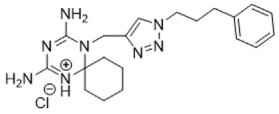	5.4	N.D	N.D
11a	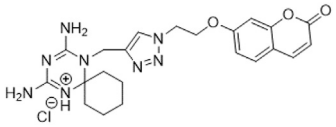	5.8	N.D	N.D
11b	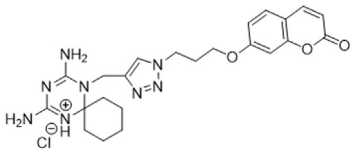	7.8	N.D	N.D
11c	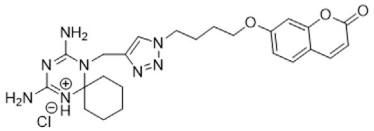	6.7	N.D	N.D
14	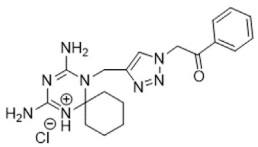	3.4	N.D	N.D
19a	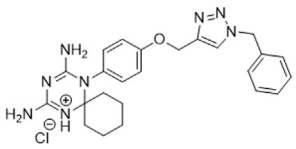	61.7	19.2	>100
19b	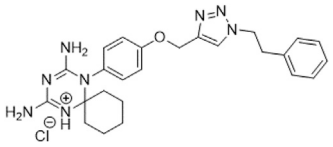	25.6	N.D	N.D
19c	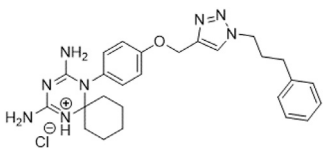	67.8	20.7	>100
20a	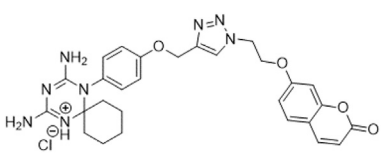	84.8	0.2	1.56

Table 1 (*continued*)

Cpd	Structure	Inhibition (%) at 25 μM	MIC_{50} (μM)	MIC_{90} (μM)
		M. bovis BCG	*M. bovis* BCG	*M. bovis* BCG
20b	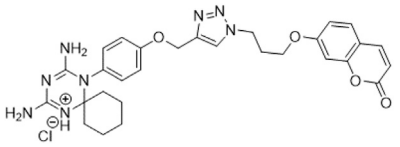	88.4	0.02	0.2
20c	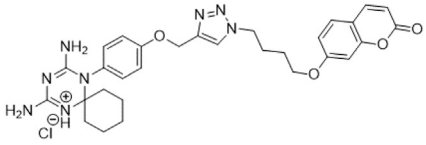	92.1	0.01–0.02	0.1
21	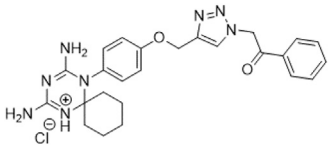	12.8	N.D	N.D

Data reported are mean values taken from 3 independent experiments.
N.D: Not determined.

Table 2
Antitubercular activity and cytotoxicity of compound **20b** and **20c**.

Cpd	MIC_{50} H37Rv (μM)	MIC_{90} H37Rv (μM)	CC_{50} HepG2 (μM)	LC_{50} RBC (μM)	SI (CC_{50}/MIC_{90})
20b	0.01	0.025	>100	>100	>4000
20c	0.01	0.025	>100	>100	>4000

Data reported are mean values taken from 3 independent experiments.

Table 3
Inhibitory activities of selected compounds on recombinant *Mtb* DHFR and human DHFR.

Cpd	IC_{50} *Mtb* DHFR (μM)	IC_{50} rh DHFR (μM)	SI (rh DHFR IC_{50}/*Mtb* DHFR IC_{50})
20b	1.34 ± 0.12	11.99 ± 1.22	~8.95
20c	0.82 ± 0.047	15.32 ± 0.45	~18.68
19c	5.82 ± 0.068	3.67 ± 0.15	~0.63
11c	>100	N.D	N.A
Methotrexate	0.035 ± 0.0024	0.0071 ± 0.0003	~0.2

N.D: Not determined.
N.A: Not available.

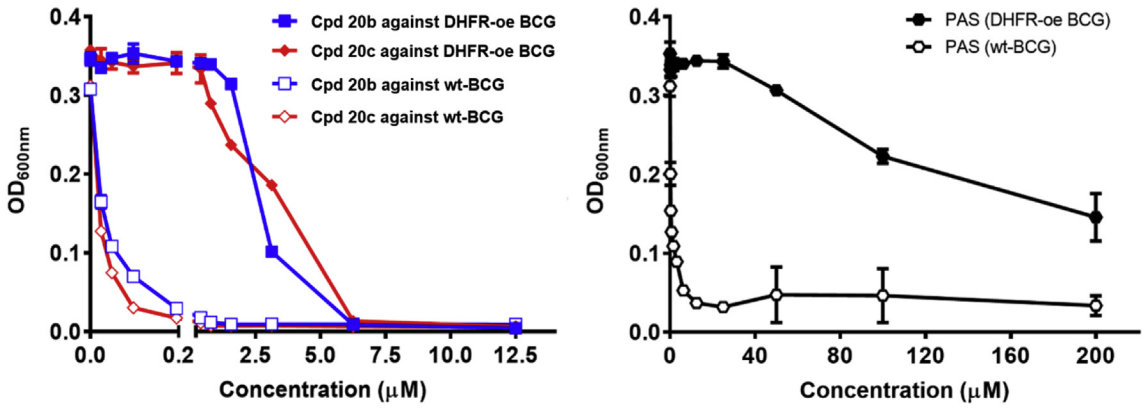

Fig. 3. (A) Dose dependent growth inhibition curves of the two most active triazaspiroalkene derivatives identified in the screen. Compounds were assayed against wild type *M. bovis* BCG (shown as clear symbols) and recombinant *M. bovis* BCG engineered to overexpress *M. bovis* BCG DHFR (shown as solid symbols). **(B)** Para-aminosalicylic acid (**PAS**) MIC shift. DHFR-oe BCG, DHFR overexpressing *M. bovis* BCG; wt-BCG, Wild type *M. bovis* BCG. OD values are the means for three replicates and error bars indicate standard error of the mean (SEM).

Table 4
Docking score of compound **20c** in *Mtb* DHFR and human DHFR.

Compound	Docking score (-log K_d)	
	Mtb DHFR	Human DHFR
20c	15.37	13.56

glycerol binding was proven to be weak and could be expelled from the binding site to expose Arg32 and Arg60 for interaction with inhibitors containing appropriate side chain. As can be seen in Fig. 4A, the coumarin ring of compound **20c** formed hydrogen bonds with Arg32 and Arg60. As a consequence, these observations and assumptions could account for the observed stronger binding affinity of compound **20c** on *Mtb* DHFR, therefore leading to the DHFR selectivity.

2.6. Preliminary in vitro DMPK study on compounds *20b* and *20c*

Finally, compounds **20b** and **20c** were also subjected to *in vitro* metabolic and pharmacokinetic profiling. Calculated parameters, such as molecular weight and the numbers of hydrogen bond donors and acceptors, are summarized in Table 5. The higher values of topological polar surface area (TPSA) of compounds **20b** and **20c** supported the good aqueous solubility of these compounds. With regard to the DMPK study, both compounds **20b** and **20c** demonstrated reasonable *in vitro* metabolic stability in rat liver microsomes. However, compound **20b** was relatively more stable with longer half-life and lower clearance in rat microsomes, as compared to compound **20c**.

In terms of drug-likeness, a majority of marketed antibacterial drugs possess different physicochemical properties in disaccordance with the Lipinski Rule [28]. The marketed gram-positive drugs possess an average TPSA of 243 Å^2 (range: 29–764 Å^2), MW of 813 (range: 290–1880), HBD of 7.1 (range: 1–29) and HBA of 16.3 (range: 2–46) [29]. The physicochemical properties of compounds **20b** and **20c** fall within these ranges. Besides, in terms of a few anti-TB agents such as rifampicin, streptomycin, amikacin, vancomycin, bedaquiline and delamanid, they also possess higher molecular weight and TPSA.

3. Conclusion

In this work, using the side chain extension approach, the 2,4-diamino-1-phenyl-1,3,5-triazaspiro[5.5]undeca-2,4-diene scaffold has been developed into novel DHFR inhibitors with attractive selectivity and potent antimycobacterial property. In terms of the potency, the 4-methyleneoxy phenyl linker when directly attached to N1 of the 1,3,5-triazaspiro[5.5]undeca-2,4-diene was found to be essential for both antimycobacterial activity and *Mtb* DHFR inhibition. The molecular docking study further corroborated the DHFR selectivity of compound **20c** for the enzyme of the pathogen and

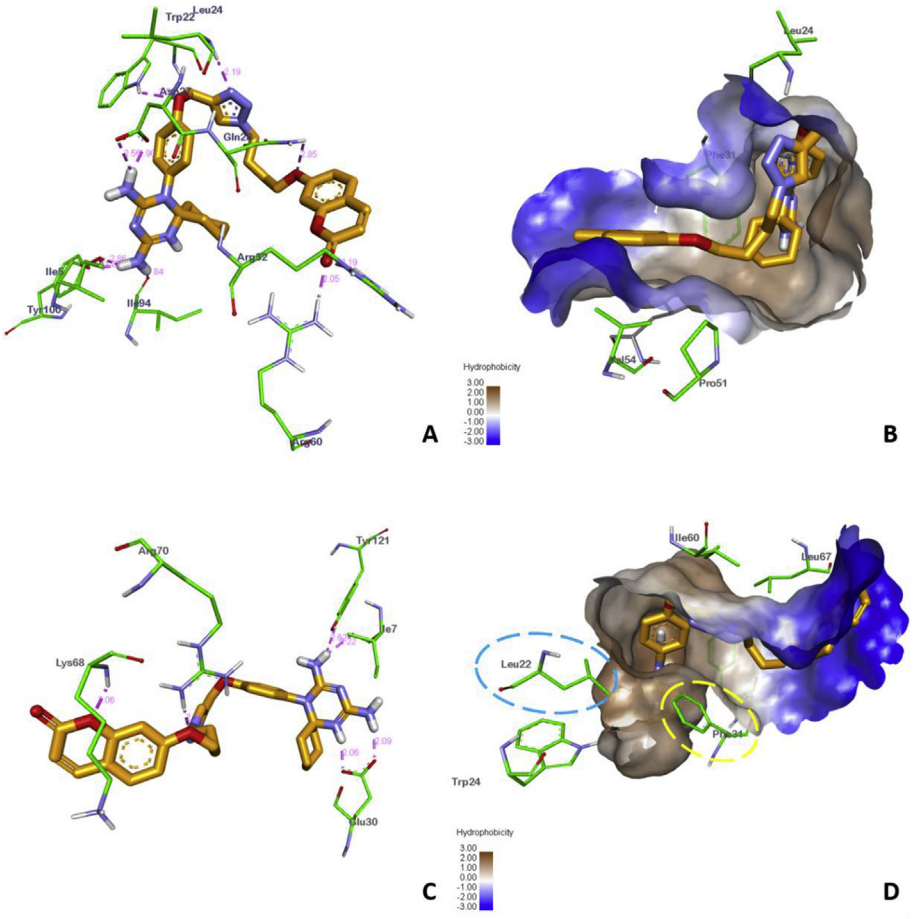

Fig. 4. Molecular docking of compound **20c**. (**A**) Optimized pose of compound **20c** at the active site of *Mtb* DHFR. (**B**) Visualization of compound **20c** interacting with the hydrophobic residues at the active site of *Mtb* DHFR. (**C**) Optimized pose of compound **20c** at the active site of human DHFR. (**B**) Visualization of compound **20c** interacting with the hydrophobic residues at the active site of human DHFR. (Brown: binding site with higher hydrophobicity; Blue: binding site with lower hydrophobicity). (For interpretation of the references to colour in this figure legend, the reader is referred to the Web version of this article.)

Table 5
In vitro characterization of compounds **20b** and **20c**.

Property	20b	20c
Mol wt	593.08	607.1
No. of HBD[a]	2	2
No. of HBA[b]	6	6
No. of rotatable bonds	9	10
cLogD[c] at pH 7.4	2.73	3.25
TPSA (Å^2)[d]	154.33	154.33
Aq solubility (μM) at pH 7.4	>100	95.83 ± 1.41
RLM $t_{1/2}$ (min, male)[e]	83.2 ± 2.9	59.0 ± 2.3
RLM $t_{1/2}$ (min, female)[e]	270.7 ± 16.4	113.5 ± 9.2
$CL_{int,\ in\ vitro}$ (μL/min/mg, male)	27.8 ± 1.0	39.2 ± 1.6
$CL_{int,\ in\ vitro}$ (μL/min/mg, female)	8.6 ± 0.5	20.4 ± 1.7

[a] HBD: hydrogen bond donors.
[b] HBA: hydrogen bond acceptors.
[c] cLogD: calculated by MarvinSketch 6.1.0.
[d] TPSA: topological polar surface area (http://www.molinspiration.com).
[e] RLM: rat liver microsomes.

unveiled the role of 1,2,3-triazole and coumarin ring in offering favourable interactions with amino acid residues at *Mtb* DHFR binding site. As mentioned above, the disconnect between enzymatic and cellular level activities might have been the result of the influence of the inclusion of His-tag on recombinant *Mtb* DHFR. In addition, further study on the role of coumarin moiety is underway to elucidate a possible secondary synergistic mechanism that may contribute to the observed cellular activity. Based on the results obtained from the biological activities, docking studies and the DMPK properties determination, compounds **20b** and **20c** are two selective *Mtb* DHFR inhibitors which have shown promise for further development into potential antitubercular agents. These two 2,4-diamino-1-phenyl-1,3,5-triazaspiro[5.5]undeca-2,4-dienes are hitherto believed to be first in demonstrating such anitmyocbacterial property through DHFR inhibition.

4. Experimental section

4.1. Chemistry

All reagents were purchased from Sigma-Aldrich (Hercules, CA, USA), Tokyo Chemical Industry (Tokyo, Japan), Alfa Aesar (Ward Hill, MA, USA), or Merck (Darmstadt, Germany) and were used directly without any purification. Thin layer chromatography (TLC) was performed using silica gel-coated aluminum plates with fluorescent indicator and visualized with UV light at 254 nm. Column chromatography was carried out on silica gel (pore size 60 Å, 230–400 mesh). ^{1}H NMR and ^{13}C NMR spectra were recorded on Bruker Ultrashield™ 400 Plus NMR spectrometer. Chemical shift values (δ) are expressed as parts per million (ppm) relative to tetramethylsilane as the internal standard. Coupling constants (J) are expressed in Hz, and splitting patterns are described as follows: s = singlet, d = doublet, t = triplet, m = multiplet, br = broad singlet, dd = doublet of doublets, dt = doublet of triplets, td = triplet of doublets, tt = triplet of triplets, ddd = doublet of doublet of doublets. ESI-MS was recorded on an AB SCIEX API 2000 Q Trap mass spectrometer. High performance liquid chromatography (HPLC) was performed for purity checking using Agilent 1100 Series HPLC on a Lichrosorb 10 RP-18 250 × 4.0 mm 10 μm column. HPLC separations were carried out using gradient elution. The initial mobile phase consisting of 80% of 0.1% w/v trifluoroacetic acid in water and 20% acetonitrile was gradually changed to 100% acetonitrile over 20 min and maintained at 100% acetonitrile for additional 2 min. All the final compounds were found to be pure up to 95% or higher.

4.1.1. 5-(prop-2-yn-1-yl)-1,3,5-triazaspiro[5.5]undeca-1,3-diene-2,4-diamine hydrochloride (**4**)

A mixture of prop-2-yn-1-amine hydrochloride (3.0 g, 32.77 mmol), cyanoguanidine (3.03 g, 36.04 mmol), cyclohexanone (3.54 g, 36.07 mmol) and concentrated HCl (0.2 mL) was refluxed with stirring under N_2 gas until a negative biguanide test was obtained. Precipitation of the product occurred either during the reaction process, or when the reaction mixture was cool down to room temperature. The solid was collected by filtration, washed with ethanol and recrystallized from 80% ethanol in H_2O. Yield: 53.7%. **^{1}H NMR** (400 MHz, DMSO-d_6): δ 8.80 (1H, br, NH), 7.62 (2H, br, NH), 7.43 (2H, br, NH), 4.32 (2H, s, CH_2), 3.42 (1H, s, alkynyl-H), 1.94–1.82 (2H, m, cyclohexyl), 1.80–1.54 (7H, m, cyclohexyl), 1.20–1.03 (1H, m, cyclohexyl) ppm. **^{13}C NMR** (100 MHz, DMSO-d_6): 157.77, 157.75, 79.65, 76.15, 71.95, 33.85, 32.77, 24.26, 21.26 ppm.

4.1.2. 1-nitro-4-(prop-2-yn-1-yloxy)benzene (**16**)

To a solution of 4-nitrophenol (1.00 g, 7.19 mmol) and K_2CO_3 (0.99 g, 7.21 mmol) in acetonitrile (50 mL) was added 3-bromoprop-1-yne (0.90 g, 7.5 mmol, 80% wt in Toluene). The reaction mixture was heated under reflux overnight. After cooling down, the reaction mixture was filtered and acetonitrile in the filtrate was removed *in vacuo*. The residue was extracted with ethyl acetate and washed with saturated NH_4Cl solution and brine. The organic layers were combined and dried over Na_2SO_4 and filtered. Removal of the solvent *in vacuo* afforded the crude product which was purified by silica gel chromatography (EA: Hexane = 1:5) to afford a white solid (1.20 g) in yield 94.6%. **^{1}H NMR** (400 MHz, DMSO-d_6): δ 8.30–8.19 (2H, m, ArH), 7.28–7.16 (2H, m, ArH), 4.99 (2H, d, J = 2.4 Hz, OCH_2), 3.68 (1H, t, J = 2.4 Hz, alkyne-CH) ppm. **^{13}C NMR** (100 MHz, DMSO-d_6): 162.83, 141.85, 126.26, 115.94, 79.64, 78.67, 56.81 ppm.

4.1.3. 4-(prop-2-yn-1-yloxy)aniline (**17**)

A mixture of **16** (1.05 g, 5.65 mmol), iron powder (2.16 g, 38.4 mmol), NH_4Cl (0.29 g, 5.08 mmol) in ethanol/water (5: 1) was stirred at reflux for 1 h. After cooling down, the reaction mixture was filtered through celite and concentrated. The residue was extracted with ethyl acetate, washed with saturated Na_2CO_3 solution and brine, and dried over Na_2SO_4 and filtered. Removal of the solvent *in vacuo* afforded the crude product which was purified by silica gel chromatography (EA: Hexane = 1:3) to afford yellow oil (0.81 g) in yield 92.9%. **^{1}H NMR** (400 MHz, DMSO-d_6): δ 6.74–6.65 (2H, m, ArH), 6.55–6.46 (2H, m, ArH), 4.66 (2H, s, NH_2), 4.59 (2H, d, J = 2.4 Hz, OCH_2), 3.47 (1H, t, J = 2.4 Hz, alkyne-CH) ppm. **^{13}C NMR** (100 MHz, DMSO-d_6): 148.99, 143.63, 116.52, 115.18, 80.48, 78.04, 56.63 ppm.

4.1.4. 5-(4-(prop-2-yn-1-yloxy)phenyl)-1,3,5-triazaspiro[5.5]undeca-1,3-diene-2,4-diamine hydrochloride (**18**)

A mixture of **17** (3.11 g, 21.14 mmol), cyanoguanidine (1.96 g, 23 mmol), ketone (24.0 mmol) and concentrated HCl (2 mL) was refluxed with stirring under N_2 gas until a negative biguanide test was obtained (18 h for cyclohexanone and 36 h for cyclopentanone). Precipitation of the product occurred either during the reaction process, or when the reaction mixture was cool down to room temperature. The solid was collected by filtration, washed with ethanol and recrystallized from 80% ethanol in H_2O. Yield 62.8%. **^{1}H NMR** (400 MHz, DMSO-d_6): δ 9.03 (1H, s, NH), 7.57 (3H, br, NH), 7.43–7.25 (2H, m, ArH), 7.22–7.02 (2H, m, ArH), 6.26 (1H, br, NH), 4.85 (2H, d, J = 2.4 Hz, OCH_2), 3.66 (1H, t, J = 2.4 Hz, alkyne-CH), 1.95–1.80 (2H, m, cyclohexyl), 1.78–1.44 (5H, m, cyclohexyl), 1.32–1.23 (2H, m, cyclohexyl), 1.00–0.84 (1H, m, cyclohexyl) ppm. **^{13}C NMR** (100 MHz, DMSO-d_6): 158.34, 158.33, 158.19, 131.80, 128.14, 116.46, 79.44, 79.11, 71.82, 56.48, 35.16, 24.42, 21.20 ppm.

*4.1.5. General procedure for the synthesis of compound **9a-9c***

A mixture of coumarin derivative (1 eq), dibromoalkane (3 eq) and K_2CO_3 (6 eq) in 50 mL acetonitrile was refluxed overnight. After the completion of reaction, excess K_2CO_3 was removed by filtration of celite and the filtrate was concentrated, washed with DCM and dried with Na_2SO_4. The residue was purified by column chromatography (EA: DCM: HEX = 1:25:25) to afford the white solid.

*4.1.5.1. 7-(2-bromoethoxy)-2H-chromen-2-one (**9a**).* Yield: 39.7%. **^{1}H NMR** (400 MHz, DMSO-d_6): δ 8.00 (1H, dd, J = 9.5, 0.6 Hz, C=CH), 7.64 (1H, d, J = 8.6 Hz, ArH), 7.03 (1H, d, J = 2.4 Hz, ArH), 6.98 (1H, dd, J = 8.6, 2.5 Hz, ArH), 6.30 (1H, d, J = 9.5 Hz, C=CH), 4.47–4.39 (2H, m, CH_2), 3.88–3.79 (2H, m, CH_2) ppm. **^{13}C NMR** (100 MHz, DMSO-d_6): 161.46, 160.67, 155.79, 144.71, 130.06, 113.25, 113.22, 113.19, 101.93, 68.85, 31.49 ppm.

*4.1.5.2. 7-(3-bromopropoxy)-2H-chromen-2-one (**9b**).* Yield: 86.9%. **^{1}H NMR** (400 MHz, DMSO-d_6): δ 7.98 (1H, dd, J = 9.5, 0.6 Hz, C=CH), 7.63 (1H, d, J = 8.5 Hz, ArH), 7.00 (1H, d, J = 2.4 Hz, 1 = ArH), 6.96 (1H, dd, J = 8.6, 2.4 Hz, ArH), 6.29 (1H, d, J = 9.4 Hz, C=CH), 4.19 (2H, t, J = 6.0 Hz, CH_2), 3.67 (2H, t, J = 6.6 Hz, CH_2), 2.27 (2H, p, J = 6.3 Hz, CH_2) ppm. **^{13}C NMR** (100 MHz, DMSO-d_6): 161.95, 160.70, 155.82, 144.73, 130.00, 113.10, 113.05, 112.96, 101.75, 66.58, 32.07, 31.44 ppm.

*4.1.5.3. 7-(4-bromobutoxy)-2H-chromen-2-one (**9c**).* Yield: 70.6%. **^{1}H NMR** (400 MHz, DMSO-d_6): δ 7.98 (1H, d, J = 9.5 Hz, C=CH), 7.62 (1H, d, J = 8.5 Hz, ArH), 6.99 (1H, d, J = 2.4 Hz, ArH), 6.94 (1H, dd, J = 8.6, 2.4 Hz, ArH), 6.28 (1H, d, J = 9.5 Hz, C=CH), 4.12 (2H, t, J = 6.3 Hz, CH_2), 3.61 (2H, t, J = 6.6 Hz, CH_2), 2.01–1.93 (2H, m, CH_2), 1.91–1.81 (2H, m, CH_2) ppm. **^{13}C NMR** (100 MHz, DMSO-d_6): 162.18, 160.74, 155.86, 144.77, 129.94, 113.19, 112.90, 112.79, 101.64, 67.91, 35.18, 29.43, 27.61 ppm.

*4.1.6. General procedure for the synthesis of azide derivatives **6a-6c**, **10a-10c** and **13***

To the corresponding bromides **5, 9a-9i**, or **12** (1.0 equivalent) in DMF, sodium azide (3.0 equivalent) was added. The resulting reaction mixture was reflux for 5 h. After cooling down to room temperature, the reaction mixture extracted with ethyl acetate (3 × 20 mL). The combined organic layers were washed with brine (1 × 10 mL) and dried over anhydrous Na_2SO_4. The crude compound was obtained *in vacuo*, and directly used in next step without further purification.

*4.1.7. General procedure for the synthesis of compound **7a-7c**, **11a-11c**, **14**, **19a-19c**, **20a-20c** and **21***

The corresponding alkyne (1.0 equivalent) and azide derivative (1.2 equivalent) were added into THF (5 mL). Sodium ascorbate (0.06 eq) was dissolved in water (4 mL), followed by copper (II) sulfate pentahydrate (0.03 eq). The reaction mixture was stirred overnight at room temperature and the reaction was monitored by TLC. After the completion of reaction, the mixture was concentrated in vacuum and dissolved in MeOH/DCM (1:9). The transparent filtrate was obtained by filtration and purified by column chromatography (MeOH/DCM = 1:50 to 1:10).

*4.1.7.1. 5-((1-benzyl-1H-1,2,3-triazol-4-yl)methyl)-1,3,5-triazaspiro[5.5]undeca-1,3-diene-2,4-diamine hydrochloride (**7a**).* Yield: 60.9%. Purity: 98.6%. **^{1}H-NMR** (400 MHz, DMSO-d_6): δ 8.66 (1H, s, NH), 8.16 (1H, s, triazolyl-H), 7.55 (2H, br, NH), 7.42–7.23 (7H, m, ArH, NH), 5.61 (2H, s, CH_2-benzyl), 4.73 (2H, s, CH_2-triazine), 1.82–1.50 (9H, m, cyclohexyl), 1.20–1.03 (1H, m, cyclohexyl) ppm. **^{13}C NMR** (100 MHz, DMSO-d_6): δ 158.42, 157.74, 143.72, 136.52, 129.19, 128.60, 128.30, 124.08, 71.91, 53.31, 38.46, 33.89, 24.19, 21.32 ppm. **ESI-MS m/z** 353.7 $(M+1)^+$.

*4.1.7.2. 5-((1-Phenethyl-1H-1,2,3-triazol-4-yl)methyl)-1,3,5-triazaspiro[5.5]undeca-1,3-diene-2,4-diamine hydrochloride (**7b**).* Yield: 66.2%. Purity: 99.1%. **^{1}H-NMR** (400 MHz, DMSO-d_6): δ 8.62 (1H, s, NH), 7.95 (1H, s, triazolyl-H), 7.54 (2H, br, NH), 7.34 (2H, br, NH), 7.30–7.09 (5H, m, ArH), 4.70 (2H, s, CH_2-triazine), 4.62 (2H, t, J = 7.1 Hz, CH_2-triazole), 3.14 (2H, t, J = 7.1 Hz, CH_2Ar), 1.83–1.47 (9H, m, cyclohexyl), 1.13 (1H, br, cyclohexyl) ppm. **^{13}C NMR** (100 MHz, DMSO-d_6): δ 158.40, 157.71, 143.28, 137.98, 129.12, 128.78, 127.01, 123.82, 71.85, 50.95, 38.45, 36.11, 33.80, 24.16, 21.32 ppm. **ESI-MS m/z** 367.7 $(M+1)^+$.

*4.1.7.3. 5-((1-(3-Phenylpropyl)-1H-1,2,3-triazol-4-yl)methyl)-1,3,5-triazaspiro[5.5]undeca-1,3-diene-2,4-diamine hydrochloride (**7c**).* Yield: 68.3%. Purity: 98.9%. **^{1}H-NMR** (400 MHz, DMSO-d_6): δ 8.70 (1H, s, NH), 8.14 (1H, s, triazolyl-H), 7.57 (2H, br, NH), 7.38 (2H, br, NH), 7.34–7.26 (2H, m, ArH), 7.19 (2H, m, ArH), 4.75 (2H, s, CH_2-triazine), 4.37 (2H, t, J = 7.0 Hz, CH_2-triazole), 2.53 (2H, t, J = 7.0 Hz, CH_2Ar), 2.11 (2H, dq, J = 9.6, 7.2 Hz, CH_2), 1.86–1.51 (9H, m, cyclohexyl), 1.23–1.07 (1H, m, cyclohexyl) ppm. **^{13}C NMR** (100 MHz, DMSO-d_6): δ 158.45, 157.76, 143.47, 141.16, 128.86, 128.73, 126.48, 123.82, 71.92, 49.45, 38.53, 33.91, 32.27, 31.82, 24.21, 21.33 ppm. **ESI-MS m/z** 381.5 $(M+1)^+$.

*4.1.7.4. 7-(2-(4-((2,4-diamino-1,3,5-triazaspiro[5.5]undeca-2,4-dien-1-yl)methyl)-1H-1,2,3-triazol-1-yl)ethoxy)-2H-chromen-2-one hydrochloride (**11a**).* Yield: 35.5%. Purity: 99.7%. **^{1}H NMR** (400 MHz, DMSO-d_6): δ 8.61 (1H, s, NH), 8.18 (1H, s, triazolyl-H), 7.99 (1H, d, J = 9.5 Hz, C=CH), 7.62 (1H, d, J = 8.6 Hz, ArH), 7.34 (3H, d, m, NH), 6.99 (1H, d, J = 2.4 Hz, Ar'H), 6.88 (1H, dd, J = 8.7, 2.4 Hz, ArH), 6.30 (1H, d, J = 9.5 Hz, C=CH), 4.81 (2H, t, J = 4.9 Hz, NCH_2), 4.75 (2H, s, triazolyl-H), 4.52 (2H, t, J = 5.0 Hz, OCH_2), 1.80–1.46 (9H, m, cyclohexyl), 1.14–1.00 (1H, m, cyclohexyl) ppm. **^{13}C NMR** (100 MHz, DMSO-d_6): δ 160.83, 160.13, 157.93, 157.22, 155.23, 144.20, 143.00, 129.58, 124.05, 112.81, 112.75, 112.58, 101.41, 71.38, 66.84, 48.48, 37.89, 33.34, 23.66, 20.82 ppm. **ESI-MS m/z** 451.4 $(M + H)^+$.

*4.1.7.5. 7-(3-(4-((2,4-Diamino-1,3,5-triazaspiro[5.5]undeca-2,4-dien-1-yl)methyl)-1H-1,2,3-triazol-1-yl)propoxy)-2H-chromen-2-one hydrochloride (**11b**).* Yield: 38.3%. Purity: 99.9%. **^{1}H NMR** (400 MHz, DMSO-d_6): δ 8.75 (1H, s, NH), 8.16 (1H, s, triazolyl-H), 8.00 (1H, d, J = 9.5 Hz, C=CH), 7.64 (1H, d, J = 8.6 Hz, ArH), 7.61–7.48 (2H, br, NH), 7.42 (2H, br, NH), 6.96 (1H, d, J = 2.4 Hz, ArH), 6.90 (1H, dd, J = 8.6, 2.4 Hz, ArH), 6.29 (1H, d, J = 9.5 Hz, C=CH), 4.74 (2H, s, CH_2-triazine), 4.55 (2H, t, J = 6.9 Hz, NCH_2), 4.07 (2H, t, J = 6.0 Hz, OCH_2), 2.30 (2H, p, J = 6.5 Hz, CH_2), 1.82–1.50 (9H, m, cyclohexyl), 1.12 (1H, m, cyclohexyl) ppm. **^{13}C NMR** (100 MHz, DMSO-d_6): δ 161.90, 160.70, 158.41, 155.80, 144.78, 143.48, 130.01, 124.05, 113.13, 113.04, 112.96, 101.65, 71.95, 65.81, 47.03, 38.48, 33.91, 29.66, 24.20, 21.28 ppm. **ESI-MS m/z** 465.4 $(M + H)^+$.

*4.1.7.6. 6-((5-(4-((2,4-Diamino-1,3,5-triazaspiro[5.5]undeca-2,4-dien-1-yl)methyl)-1H-1,2,3-triazol-1-yl)pentyl)oxy)-2H-chromen-2-one hydrochloride (**11c**).* Yield: 46.9%. Purity: 99.2%. **^{1}H NMR** (400 MHz, DMSO-d_6): δ 8.68 (1H, br, NH), 8.14 (1H, s, triazolyl-H), 7.99 (1H, d, J = 9.5 Hz, C=CH), 7.62 (1H, d, J = 8.6 Hz, ArH), 7.58 (2H, br, NH), 7.37 (2H, br, NH), 6.97 (1H, d, J = 2.4 Hz, ArH), 6.92 (1H, dd, J = 8.6, 2.4 Hz, ArH), 6.28 (1H, d, J = 9.5 Hz, C=CH), 4.74 (2H, s, CH_2-triazine), 4.45 (2H, t, J = 7.0 Hz, NCH_2), 4.09 (2H, t, J = 6.4 Hz, OCH_2), 1.97 (2H, p, J = 7.1 Hz, CH_2), 1.84–1.50 (11H, m, cyclohexyl, CH_2), 1.13 (1H, m, cyclohexyl) ppm. **^{13}C NMR** (100 MHz, DMSO-d_6): δ 162.14, 160.74, 158.43, 157.74, 155.85, 144.79, 143.40, 129.97, 123.88, 113.15, 112.92, 112.81, 101.63, 71.91, 68.07, 49.53, 38.50, 33.89, 26.94, 25.87, 24.20, 21.31 ppm. **ESI-MS m/z** 479.4 $(M + H)^+$.

*4.1.7.7. 2-[4-(2,4-Diamino-1,3,5-triaza-spiro[5.5]undeca-2,4-dien-1-ylmethyl)-[1,2,3]triazol-1-yl]-1-phenyl-ethanone hydrochloride (**14**).* Yield: 63.4%. Purity: 95.9%. **^{1}H NMR** (400 MHz, DMSO-d_6): δ 8.70 (1H, s, NH), 8.09 (1H, s, triazolyl-H), 8.06 (2H, d, J = 8.0, 0.9 Hz, ArH), 7.74 (1H, t, J = 6.8 Hz, ArH), 7.63 (2H, s, NH), 7.61 (2H, t, J = 7.7 Hz, ArH), 7.38 (2H, s, NH), 6.19 (2H, s, $COCH_2$), 4.82 (2H, s, triazolyl-H), 1.97–1.89 (2H, m, cyclohexyl), 1.87–1.54 (7H, m, cyclohexyl), 1.20–1.03 (1H, m, cyclohexyl) ppm. **^{13}C NMR** (100 MHz, DMSO-d_6): δ 192.61, 158.44, 157.80, 143.38, 134.68, 134.62, 129.44, 128.63, 125.70, 71.95, 56.41, 38.40, 33.87, 24.21, 21.36 ppm. **ESI-MS m/z** 381.4 $(M + H)^+$.

*4.1.7.8. 5-(4-((1-benzyl-1H-1,2,3-triazol-4-yl)methoxy)phenyl)-1,3,5-triazaspiro[5.5]undeca-1,3-diene-2,4-diamine hydrochloride (**19a**).* Yield: 62.7%. Purity: 99.3%. **^{1}H NMR** (400 MHz, DMSO-d_6): δ 8.99 (1H, s, NH, exchangeable proton), 8.33 (1H, s, triazoyl-H), 7.54 (2H, br, NH), 7.41–7.32 (5H, m, Ar'H), 7.26 (2H, d, J = 8.9 Hz, ArH), 7.16 (2H, d, J = 8.9 Hz, ArH), 6.22 (1H, s, NH), 5.63 (2H, s, OCH_2), 5.18 (2H, s, CH_2), 1.87–1.84 (2H, m, cyclohexyl), 1.66–1.50 (5H, m, cyclohexyl), 1.31–1.23 (2H, m, cyclohexyl), 0.96–0.86 (1H, m, cyclohexyl) ppm. **^{13}C NMR** (100 MHz, DMSO-d_6): δ 159.18, 158.31, 158.24, 143.11, 136.44, 131.79, 129.23, 128.65, 128.45, 127.78, 125.29, 116.43, 71.83, 61.88, 53.35, 35.17, 24.42, 21.21 ppm. **ESI-MS m/z** 445.7 $(M + H)^+$.

*4.1.7.9. 5-(4-((1-(2-Phenylethyl)-1H-1,2,3-triazol-4-yl)methoxy)phenyl)-1,3,5-triazaspiro[5.5]undeca-1,3-diene-2,4-diamine hydrochloride (**19b**).* Yield: 57.0%. Purity: 95.6%. **^{1}H NMR** (400 MHz, DMSO-d_6): δ 8.99 (1H, s, NH), 8.20 (1H, s, triazoyl-H), 7.54 (3H, br, NH), 7.29–7.14 (9H, m, ArH and Ar'H), 7.23 (1H, s, Ar'H), 7.18 (4H, dt, J = 15.2, 6.2 Hz, Ar'H), 6.21 (1H, s, NH), 5.16 (2H, s, OCH_2), 4.64 (2H, t, J = 7.3 Hz, NCH_2), 3.17 (2H, t, J = 7.3 Hz, CH_2Ar'H), 1.86–1.85 (2H, m, cyclohexyl), 1.67–1.50 (5H, m, cyclohexyl), 1.32–1.23 (2H, m, 2H, cyclohexyl), 0.95–0.95 (1H, m, cyclohexyl) ppm. **^{13}C NMR** (100 MHz, DMSO-d_6): δ 159.17,158.31, 158.24, 142.64, 138.03, 131.79, 129.12, 128.87, 127.75, 127.04, 125.06, 116.47, 71.83, 61.93, 50.94, 36.12, 35.18, 24.41, 21.21 ppm. **ESI-MS m/z** 459.7 $(M + H)^+$.

*4.1.7.10. 5-(4-((1-(3-Phenylpropyl)-1H-1,2,3-triazol-4-yl)methoxy)phenyl)-1,3,5-triazaspiro[5.5]undeca-1,3-diene-2,4-diamine hydrochloride (**19c**).* Yield: 47.1%. Purity: 99.4%. **^{1}H NMR** (400 MHz, DMSO-d_6): δ 9.02 (1H, s, NH), 8.31 (1H, s, triazolyl-H), 7.55 (3H, br, NH), 7.31–7.16 (9H, m, ArH and Ar'H), 6.22 (1H, br, NH), 5.19 (1H, s, OCH_2), 4.39 (2H, J = 7.1 Hz, NCH_2), 2.59–2.55 (2H, m, Ar'CH_2), 2.19–2.11 (2H, m, Ar'CH_2), 1.87–1.84 (2H, m, cyclohexyl), 1.70–1.52 (5H, m, cyclohexyl), 1.31–1.23 (2H, m, cyclohexyl), 0.94–0.84 (1H, m, cyclohexyl) ppm. **^{13}C NMR** (100 MHz, DMSO-d_6): δ 159.18, 158.33, 158.23, 142.81, 141.15, 131.79, 128.86, 128.76, 127.77, 126.48, 125.07, 116.47, 71.83, 62.96, 49.43, 35.18, 32.33, 31.77, 24.42, 21.19 ppm. **ESI-MS m/z** 473.4 $(M + H)^+$.

*4.1.7.11. 7-(2-(4-((4-(2,4-diamino-1,3,5-triazaspiro[5.5]undeca-2,4-dien-1-yl)phenoxy)methyl)-1H-1,2,3-triazol-1-yl)ethoxy)-2H-chromen-2-one hydrochloride (**20a**).* Yield: 66.5%. Purity: 99.5%. **^{1}H NMR** (400 MHz, DMSO-d_6): δ 8.93 (1H, s, NH), 8.37 (1H, s, triazolyl-H), 8.00 (1H, d, J = 9.5 Hz, C=CH), 7.63 (1H, d, J = 8.6 Hz, Ar'H), 7.44 (2H, br, NH), 7.26 (2H, d, J = 8.9 Hz, ArH), 7.17 (2H, d, J = 9.0 Hz, ArH), 7.03 (1H, d, J = 2.4 Hz, Ar'H), 6.94 (1H, dd, J = 8.6, 2.5 Hz, Ar'H), 6.30 (1H, d, J = 9.5 Hz, C=CH), 6.23 (1H, br, NH), 5.19 (2H, s, OCH_2), 4.84 (2H, t, J = 5.0 Hz, CH_2), 4.55 (2H, t, J = 5.0 Hz, CH_2), 1.87–1.84 (2H, m, cyclohexyl), 1.70–1.52 (5H, m, cyclohexyl), 1.30–1.24 (2H, m, cyclohexyl), 0.94–0.84 (1H, m, cyclohexyl) ppm. **^{13}C NMR** (100 MHz, DMSO-d_6): 161.32, 160.64, 159.18, 158.27, 158.22, 155.73, 144.70, 142.88, 131.78, 130.06, 127.75, 125.81, 116.42, 113.31, 113.26, 113.14, 101.99, 71.79, 67.30, 61.83, 49.36, 35.14, 24.39, 21.21 ppm. **ESI-MS m/z** 543.4 $(M+1)^+$.

*4.1.7.12. 7-(3-(4-((4-(2,4-diamino-1,3,5-triazaspiro[5.5]undeca-2,4-dien-1-yl)phenoxy)methyl)-1H-1,2,3-triazol-1-yl)propoxy)-2H-chromen-2-one hydrochloride (**20b**).* Yield: 41.2%. Purity: 99.1%. **^{1}H NMR** (400 MHz, DMSO-d_6): δ 9.04 (1H, s, NH), 8.34 (1H, s, triazolyl-H), 8.00 (1H, d, J = 9.5 Hz, C=CH), 7.63 (1H, d, J = 8.6 Hz, ArH), 7.56 (2H, s, NH), 7.26 (2H, d, J = 8.9 Hz, ArH), 7.17 (2H, d, J = 9.0 Hz, Ar), 7.01–6.88 (2H, m, Ar'H), 6.29 (1H, d, J = 9.5 Hz, C=CH), 6.22 (1H, s, NH), 5.18 (2H, s, OCH_2), 4.58 (2H, t, J = 6.9 Hz, CH_2), 4.11 (2H, t, J = 6.0 Hz, CH_2), 2.33 (2H, p, J = 6.4 Hz, CH_2), 1.87–1.84 (2H, m, cyclohexyl), 1.74–1.47 (5H, m, cyclohexyl), 1.29–1.24 (2H, m, cyclohexyl), 0.94–0.84 (1H, m, cyclohexyl) ppm. **^{3}C NMR** (100 MHz, DMSO-d_6): 161.92, 160.71, 159.18, 158.32, 158.21, 155.79, 144.77, 142.81, 131.79, 129.99, 127.76, 125.36, 116.43, 113.12, 113.04, 112.96, 101.74, 71.83, 65.93, 61.92, 47.10, 35.18, 29.70, 24.43, 21.19 ppm. **ESI-MS m/z** 557.4 $(M+1)^+$.

*4.1.7.13. 7-(4-(4-((4-(2,4-diamino-1,3,5-triazaspiro[5.5]undeca-2,4-dien-1-yl)phenoxy)methyl)-1H-1,2,3-triazol-1-yl)butoxy)-2H-chromen-2-one hydrochloride (**20c**).* Yield: 66.6%. Purity: 99.0%. **^{1}H NMR** (400 MHz, DMSO-d_6): δ 8.98 (1H, br, NH), 8.31 (1H, s, triazolyl-H), 7.99 (1H, d, J = 9.5 Hz, C=CH), 7.63 (1H, d, J = 8.6 Hz, Ar'H), 7.53 (3H, br, NH), 7.27 (2H, d, J = 8.9 Hz, ArH), 7.17 (2H, d, J = 9.0 Hz, ArH), 7.03–6.91 (2H, m, Ar'H), 6.28 (1H, d, J = 9.5 Hz, C=CH), 6.22 (1H, br, NH), 5.18 (2H, s, OCH_2), 4.47 (2H, t, J = 7.0 Hz, CH_2), 4.11 (2H, t, J = 6.4 Hz, CH_2), 2.07–1.93 (2H, m, CH_2), 1.88–1.84 (2H, m, cyclohexyl), 1.79–1.65 (2H, m, CH_2), 1.68–1.47 (5H, m, cyclohexyl), 1.29–1.25 (2H, m, cyclohexyl), 1.00–0.83 (1H, m, cyclohexyl) ppm. **^{13}C NMR** (100 MHz, DMSO-d_6): 162.15, 160.74, 159.19, 158.29, 155.85, 144.79, 142.77, 131.80, 129.96, 127.76, 125.14, 116.43, 113.17, 112.93, 112.81, 101.66, 71.81, 68.07, 61.93, 49.55, 36.16, 26.92, 25.93, 24.41, 21.21 ppm. **ESI-MS m/z** 571.4 $(M+1)^+$.

*4.1.7.14. 2-(4-((4-(2,4-diamino-1,3,5-triazaspiro[5.5]undeca-2,4-dien-1-yl)phenoxy)methyl)-1H-1,2,3-triazol-1-yl)-1-phenylethanone hydrochloride (**21**).* Yield: 43.8%. Purity: 98.2%. **^{1}H NMR** (400 MHz, DMSO-d_6): δ 9.00 (1H, s, NH), 8.24 (1H, s, triazolyl-H), 8.08 (2H, d, J = 7.1 Hz, Ar'H), 7.75 (1H, t, J = 7.4 Hz, Ar'H), 7.62 (2H, t, J = 7.6 Hz, Ar'H), 7.52 (3H, br, NH), 7.28 (2H, d, J = 8.9 Hz, Ar), 7.21 (2H, d, J = 9.0 Hz, ArH), 6.23 (2H, s, $NCH_2C{=}O$), 5.25 (2H, s, OCH_2), 1.89–1.84 (2H, m, cyclohexyl), 1.65–1.57 (5H, m, cyclohexyl), 1.39–1.21 (2H, m, cyclohexyl), 0.99–0.85 (1H, m, cyclohexyl) ppm. **^{13}C NMR** (100 MHz, DMSO-d_6): 192.61, 159.24, 158.26, 158.19, 142.72, 134.74, 134.56, 131.81, 129.46, 128.64, 127.78, 126.94, 116.46, 71.77, 61.90, 56.38, 35.11, 24.39, 21.25 ppm. **ESI-MS m/z** 473.5 $(M+1)^+$.

4.2. Strains and growth condition

Liquid and solid cultures of *M. bovis* BCG (Pasteur 1173P2) and *Mycobacterium tuberculosis* H37Rv (ATCC 27294) were grown as described previously [25]. Liquid cultures were grown on rollers using filter sterilized Middlebrook 7H9 broth (BD Difco) supplemented with 0.5% albumin, 0.2% dextrose, 0.0003% catalase, 0.085% sodium chloride, 0.2% glycerol and 0.05% Tween 80. Solid cultures were grown on Middlebrook 7H11 agar (BD Difco) supplemented with 0.006% oleic acid, 0.5% albumin, 0.2% dextrose, 0.0003% catalase, 0.085% sodium chloride and 0.5% glycerol. HepG2 (ATCC HB.8065) cells were cultured at 37 °C with 5% CO_2 atmosphere in DMEM media (Gibco) complemented with 10% heat-inactivated FBS (Gibco), penicillin (100 U/mL, Gibco) and streptomycin (100 μg/mL, Gibco). For hemolysis assay, red blood cells were obtained from Interstate Blood Bank, Inc. Laboratory, USA.

4.3. MIC determination

Minimum inhibitory concentrations (MICs) were determined by the broth microdilution method as described previously [23–25]. Briefly, mycobacterial cells were grown in roller bottles until OD_{600} reached mid log phase (0.4–0.6). The cultures were then diluted to a starting bacterial OD_{600} of 0.01. Compounds (dissolved in 90% DMSO) were serially diluted 2 fold in 100 μL volume in 96 well microtiter plates (Flat bottom polystyrene, Corning Inc.). Then, bacterial suspensions were dispensed to each well in 100 μL volume making the final volume and cell density 200 μL and 5×10^5 CFU/mL, respectively. Plates were then aseptically sealed with Breathe-Easy sealing membrane (Sigma), placed in a humidified lock-lock box and incubated at 37^{O}C for 10 days with shaking at 80 rpm. Growth inhibition was measured by reading optical density (OD_{600}) using TECAN infinite M200Pro microplate reader (TECAN, Salzburg, Austria) and the inhibitory activities were interpreted based on the MIC_{50} and MIC_{90} values, the minimum concentrations that inhibit 50% and 90% of bacterial growth. Rifampicin and untreated culture containing DMSO were included as inhibition and growth controls, respectively.

4.4. Cytotoxicity and hemolysis assay

The *in vitro* cytotoxicity effect was determined using CellTiter 96® AQ_{ueous} One Solution Cell Proliferation Assay (MTS) kit (Promega). In the assay, human hepatic cell lines (HepG2, ATCC HB-8065) were exposed to two fold serially diluted compound concentrations and viability was assessed by measuring the decrease in the absorbance at 490 nm with a TECAN M200Pro microplate reader. Absorbance was plotted as a function of compound concentrations and the minimum cidal concentration corresponding to 50% reduction in cell viability was determined. Triton X-100 was used as a cytotoxic positive control.

Lytic effect on red blood cells was also evaluated following a modified procedure described previously [30]. Briefly, cells were washed with PBS, re-suspended to a final cell number of 10^6/mL and incubated with test compounds for 24 h. After exposure, the red blood cells were subsequently centrifuged (1000 g for 10 min) and absorbance of the supernatant was read at 540 nm. PBS and 0.1% Triton X-100 were included as negative and positive controls, respectively.

4.5. DHFR inhibition assay

Potassium phosphate buffer (0.15 M, pH 7) was used for all the DHFR assays. A solution of NADPH (2 mg/mL, 2 mM) in potassium phosphate buffer (0.15 M, pH 7) was prepared immediately before use and kept on ice. A solution of dihydrofolate (DHF) (1 mg/mL, 2 mM) was prepared immediately before use by suspending DHF in deionized water and adding a drop of sodium hydroxide (1 M) solution to aid dissolution. The DHF solution was protected from light and kept on ice. Recombinant human DHFR was purchased from Sigma-Aldrich (St. Louis, MO, USA). Recombinant *Mtb* DHFR was supplied by Protein Production Platform, School of Biological Sciences, Nanyang Technological University. The test compounds were dissolved in DMSO and diluted to the appropriate concentrations.

The assay was conducted by mixing the appropriate volumes of phosphate buffer, NADPH, DHF, recombinant human or *Mtb* DHFR and test compound in a 1 mL quartz cuvette to obtain a solution containing 50 μM DHF, 60 μM NADPH, 0.15 M phosphate buffer (pH 7), 1.5×10^{-3} units of recombinant human DHFR or 0.3 ng/mL *Mtb* DHFR and various concentrations of the assayed compounds. For each experiment, a control reading was taken in which 10 μL of DMSO was added instead of the test compound. A blank reading was also taken, in which the DHFR enzyme was omitted and 10 μL of DMSO was added instead of the test compound. The assay was carried out at room temperature, and the rate of consumption of NADPH during the conversion of DHF to tetrahydrofolate (THF) was monitored by taking absorbance readings at 340 nm every 30 s over 6 min using a Hitachi U-1900 UV/visible spectrophotometer. A graph of absorbance readings versus time was plotted and the slope of the graph over the linear range from 30 s to 6 min was taken to represent the rate of reaction. The percentage inhibition at each concentration of inhibitor was calculated using the following formulae:

$$\text{Activity} = \frac{\text{Slope of inhibited enzyme}}{\text{Slope of uninhibited enzyme}}$$

$$\text{Inhibition (\%)} = 100 - \text{Activity}$$

Graphs of percentage inhibition against logarithmic concentration were plotted for each compound and IC50 values were calculated using GraphPad Prism Version 5.01.

4.6. Construction of DHFR overexpressing M. bovis BCG strain

We used mycobacterial shuttle vector pMV262 (conferring kanamycin resistance) to overexpress DHFR in *M. bovis* BCG under the control of a constitutive promoter hsp60 [26]. The coding region of *dfrA* was first PCR amplified (KOD polymerase, Toyobo Life Science) with primers containing *Bam*HI and *Eco*RI restriction sites (Forward *Bam*HI; ccgggatccATGGTGGGGCTGATCTGGG and Reverse *Eco*RI; ccggaattcTCATGAGCGGTGGTAGCTGT) and cloned inframe (*Not*I-*Bam*HI). Purified plasmid DNA from *E. coli* DH5α was electroporated to *M. Bovis* BCG as previously described [31]. The amount of DHFR overexpression was quantified at the transcript level by using qRT-PCR (SuperScript® III) [32]. RNA from *M. Bovis BCG* wild type was isolated from the equivalent of 20 mL of cells at $OD_{60nm} = 0.4$. Cultures were centrifuged, re-suspended in TRIzol (Invitrogen) and subjected to bead beating by using FastPrep-24™ 5G Instrument (MP Biomedicals, 2 × 45 s each, 5 min on ice between pulses). RNA was purified using PureLink™ RNA Mini Kit with TURBO DNA-free kit (Invitrogen). cDNA was created from 1 μg of total RNA with the SuperScript III First Strand Synthesis System (Invitrogen) by using random primers. Quantitative PCR was performed with the FastStart Essential DNA Green Master (Roche) using the LightCycler 96 Real-Time PCR System (Roche) by using primers for *dfrA* (Forward; GTCGACCTCGGTAACCTCAC, Reverse; TGAGGTTGTCGGTTCACTCG) and 16S RNA (Forward; ATGACGGCCTTCGGGTTGTAA, Reverse; CGGCTGCTGGCACGTAGTTG), respectively. Relative expression (ΔΔCq) was calculated as described by using 16S RNA as reference [33]. Para-aminosalicylic acid (PAS) was used as a positive control [34].

4.7. Molecular docking study

Molecular docking is another commonly used virtual screening method for drug discovery. Unlike machine learning, it is a target-based method to estimate the binding affinity between ligand and target. In this study, molecular docking screening was conducted using the Surflex-Dock module in SYBYL–X 2.1 (Tripos associate Inc., St. Louis, MO, USA).

For small molecule preparation, the 3D structure of the compounds was minimized in SYBYL-X 2.1. The partial atomic charge was calculated by the Gasteiger Huckel method and energy minimization was performed using the Tripos force field with a

distance-dependent dielectric and the Powell conjugate gradient algorithm convergence criteria.

The 3D structure of *Mtb* DHFR (PDB: 1DF7) and human DHFR (PDB: 2W3M) was obtained from protein data bank (PDB). Generally, During protein preparation, the co-crystallized ligand was first removed from the structure together with the water molecules. H atoms were then added and side chains were fixed. Protomol generation parameters were threshold 0.5 and boat 0 for both enzymes. Surflex-Dock used an empirically scoring function based on the binding affinity, which was expressed in -log K_d involving hydrophobicity, polarity, repulsion, entropy, solvation and crash terms. The higher the score is, the more tightly the ligand binds to receptor. The top 20 poses of each ligand were obtained and analyzed for their interactions with the protein.

4.8. DMPK study

The rat liver microsome (RLM) stability and solubility assays were carried out at Drug Development Unit (DDU), National University of Singapore (NUS).

For determining solubility, the compound was serially diluted from a 10 mM stock in DMSO to a series of final concentrations, consisting of 100 μM, 50 μM, 25 μM, 12.5 μM, 6.25 μM and 3.13 μM in an aqueous buffer (45 mM ethanolamine, 45 mM potassium dihydrogen phosphate, 45 mM potassium acetate, pH 7.4). Following an incubation of 90 min at room temperature, the aqueous dilution was filtrated into a 96-well UV plate. After filtration, 80 μL of filtrate was transferred from each well to another well in a 96-well UV plate. 20 μL of acetonitrile was added to each well. This will give the 80:20 buffer:acetonitrile composition of the sample solutions. After that, the sample solutions were diluted by adding another 200 μL of buffer. The absorbance of the solutions was read at 330 nm.

Metabolic stability was measured in liver microsomes from male and female rats by LC-MS-based measuring 3 μM over time up to 45 min at 37 °C. Incubation mixtures consisted of 7.5 μL of 20 mg/mL FRLM and MRLM (final: 0.3 mg microsome protein/mL), 2.5 μL of 600 μM compound in acetonitrile (final: 3 μM), 440 μL of 0.1 M phosphate buffer (pH 7.4). The mixture was first shaken for 5 min for pre-incubation in a shaking water bath at 37 °C. Reaction was initiated by adding 50 μL of 10 mM NADPH to obtain a final concentration of 1 mM NADPH in the mixture. The total volume of the reaction mixture was 500 μL. For metabolic stability studies, aliquots of 50 μL of the incubation sample mixture were collected at 0, 5, 10, 15, 30, and 45 min. After collection of samples, the reaction was terminated with 100 μL of chilled acetonitrile containing the internal standard. The mixture was then centrifuged at 10,000 × g to remove the protein and the supernatant was subsequently applied to LC-MS/MS analysis. Based on compound half-life, *in vitro* intrinsic clearance CL_{int} was calculated.

Conflicts of interest

All authors have given approval to the final version of the manuscript and declare that they have no conflict of interest.

Acknowledgments

This work was supported by:

(i) The National University of Singapore Academic Research Fund Tier 1 R-148-000-205-112, which was awarded to W.K. Chui.

(ii) The Singapore Ministry of Health's National Medical Research Council's TCR Flagship grant NMRC/TCR/011-NUHS/2014 which was awarded to T. Dick. The grant contributes to part of Singapore Programme of Research Investigating New Approaches to Treatment of Tuberculosis (SPRINT-TB; www.sprinttb.org) led by Nick Paton.

(iii) The NUS Medicine BSL-3 Core Facility, National University of Singapore, National University Health System and the Singapore Ministry of Health, National Medical Research Council, Center Grant 'MINE', Research Core #4 (NMRC/CG/013/2013).

(iv) Bill Jacobs from the Albert Einstein College of Medicine for sharing his plasmid pMV262.

References

[1] M. Raviglione, G. Sulis, Tuberculosis, 2015: burden, challenges and strategy for control and elimination, Infect. Dis. Rep. 8 (2016) 6570.
[2] World Health Organization (WHO), Global Tuberculosis Report, 2015. http://www.who.int/tb/publications/global_report/en/.
[3] M. Pieroni, D. Machado, E. Azzali, S. Santos Costa, I. Couto, G. Costantino, M. Viveiros, Rational design and synthesis of thioridazine analogues as enhancers of the antituberculosis therapy, J. Med. Chem. 58 (2015) 5842–5853.
[4] World Health Organization (WHO), Global Tuberculosis Report, 2015. http://www.who.int/tb/publications/global_report/en/.
[5] V. Dartois, The path of anti-tuberculosis drugs: from blood to lesions to mycobacterial cells, Nat. Rev. Microbiol. 12 (2014) 159–167.
[6] E.W. Orenstein, S. Basu, N.S. Shah, J.R. Andrews, G.H. Friedland, A.P. Moll, N.R. Gandhi, A.P. Galvani, Treatment outcomes among patients with multidrug-resistant tuberculosis: systematic review and meta-analysis, Lancet Infect. Dis., 9 153–161.
[7] I.M. Kompis, K. Islam, R.L. Then, DNA and RNA synthesis: antifolates, Chem. Rev. 105 (2005) 593–620.
[8] D.L. Wright, A.C. Anderson, Antifolate agents: a patent review (2006 – 2010), Expert Opinion on Therapeutic Patents, 21 (2011) 1293–1308.
[9] S. Hawser, S. Lociuro, K. Islam, Dihydrofolate reductase inhibitors as antibacterial agents, Biochem. Pharmacol. 71 (2006) 941–948.
[10] L. Arundhati Chandrashekhar, M. Deepak Amarnath, K. Tengku Karmila, B. Sanjib, D. Mariam Sohel, Repositioning of DHFR inhibitors, Curr. Top. Med. Chem. 16 (2016) 2125–2143.
[11] Molly R. Nixon, Kurt W. Saionz, M.-S. Koo, Michael J. Szymonifka, H. Jung, Justin P. Roberts, M. Nandakumar, A. Kumar, R. Liao, T. Rustad, James C. Sacchettini, Kyu Y. Rhee, Joel S. Freundlich, David R. Sherman, Folate pathway disruption leads to critical disruption of methionine derivatives in Mycobacterium tuberculosis, Chem. Biol. 21 (2014) 819–830.
[12] A. Kumar, A. Guardia, G. Colmenarejo, E. Pérez, R.R. Gonzalez, P. Torres, D. Calvo, R.M. Gómez, F. Ortega, E. Jiménez, R.C. Gabarro, J. Rullás, L. Ballell, D.R. Sherman, A Focused screen identifies antifolates with activity on *Mycobacterium tuberculosis*, ACS Infect. Dis. 1 (2015) 604–614.
[13] N.R. Tawari, S. Bag, A. Raju, A.C. Lele, R. Bairwa, M.K. Ray, M.G.R. Rajan, L.U. Nawale, D. Sarkar, M.S. Degani, Rational drug design, synthesis and biological evaluation of dihydrofolate reductase inhibitors as antituberculosis agents, Future Med. Chem. 7 (2015) 979–988.
[14] W. Zhou, E.W. Scocchera, D.L. Wright, A.C. Anderson, Antifolates as effective antimicrobial agents: new generations of trimethoprim analogs, MedChemComm 4 (2013) 908–915.
[15] A.C. Anderson, D.L. Wright, Antifolate agents: a patent review (2010 – 2013), Expert Opin. Ther. Pat. 24 (2014) 687–697.
[16] X. Ma, S.-T. Tan, C.-L. Khoo, H.-M. Sim, L.-W. Chan, W.-K. Chui, Synthesis and antimicrobial activity of N1-benzyl or N1-benzyloxy-1,6-dihydro-1,3,5-triazine-2,4-diamines, Bioorg. Med. Chem. Lett. 21 (2011) 5428–5431.
[17] P. Ong, Triazaspiroalkenes as Potential Inhibitors of Dihydrofolate Reductase, Singapore, 2009.
[18] R. Li, R. Sirawaraporn, P. Chitnumsub, W. Sirawaraporn, J. Wooden, F. Athappilly, S. Turley, W.G.J. Hol, Three-dimensional structure of *M. tuberculosis* dihydrofolate reductase reveals opportunities for the design of novel tuberculosis drugs, J. Mol. Biol. 295 (2000) 307–323.
[19] E.F.F. da Cunha, T.d.C. Ramalho, R.B. de Alencastro, E.R. Maia, Interactions of 5-deazapteridine derivatives with Mycobacterium tuberculosis and with human dihydrofolate reductases, J. Biomol. Struct. Dyn. 22 (2004) 119–130.
[20] E.J. Modest, Chemical and biological studies on 1,2-dihydro-s-triazines. II. Three-component synthesis, J. Org. Chem. 21 (1956) 1–13.
[21] U.H. Manjunatha, P.W. Smith, Perspective: challenges and opportunities in TB drug discovery from phenotypic screening, Bioorg. Med. Chem. 23 (2015) 5087–5097.
[22] J. Magdalena, P. Supply, C. Locht, Specific differentiation between *Mycobacterium bovis* BCG and virulent strains of the *Mycobacterium tuberculosis* complex, J. Clin. Microbiol. 36 (1998) 2471–2476.
[23] J.M. Andrews, Determination of minimum inhibitory concentrations, J. Antimicrob. Chemother. 48 (2001) 5–16.
[24] D. Blanco-Ruano, D.M. Roberts, R. Gonzalez-Del-Rio, D. Álvarez, M.J. Rebollo, E. Pérez-Herrán, A. Mendoza, Antimicrobial susceptibility testing for Mycobacterium sp, Mycobact. Protoc. (2015) 257–268.
[25] S.B. Lakshminarayana, T.B. Huat, P.C. Ho, U.H. Manjunatha, V. Dartois, T. Dick, S.P. Rao, Comprehensive physicochemical, pharmacokinetic and activity profiling of anti-TB agents, J. Antimicrob. Chemother. 70 (3) (2014) 857–867.

[26] C. Stover, V. De La Cruz, New uses of BCG for recombinant vaccines, Nature 351 (1991) 456.
[27] W. Hong, Z. Chang, Y. Wang, T. Sun, J. Pu, I.C. Paterson, H. Wang, The influence of glycerol on the binding of methotrexate to Mycobacterium tuberculosis dihydrofolate reductase: a molecular modelling study, Mol. Simul. 41 (2015) 1540–1545.
[28] J.-P. Ebejer, M.H. Charlton, P.W. Finn, Are the physicochemical properties of antibacterial compounds really different from other drugs? J. Cheminformatics 8 (2016) 30.
[29] S.B. Lakshminarayana, T.B. Huat, P.C. Ho, U.H. Manjunatha, V. Dartois, T. Dick, S.P.S. Rao, Comprehensive physicochemical, pharmacokinetic and activity profiling of anti-TB agents, J. Antimicrob. Chemother. 70 (2015) 857–867.
[30] W. Moreira, D.B. Aziz, T. Dick, Boromycin kills mycobacterial persisters without detectable resistance, Front. Microbiol. 7 (2016) 199.
[31] T. Parish, N.G. Stoker, Electroporation of mycobacteria, Mycobact. Protoc. (1998) 129–144.
[32] Y. Yamada, T. Dick, Mycobacterial caseinolytic protease gene Regulator ClgR is a substrate of caseinolytic protease, mSphere 2 (2017).
[33] P. MW, A new mathematical model for relative quantification in real-time RT-PCR, Nucleic Acids Res. 29 (2001).
[34] J. Zheng, E.J. Rubin, P. Bifani, V. Mathys, V. Lim, M. Au, J. Jang, J. Nam, T. Dick, J.R. Walker, para-Aminosalicylic acid is a prodrug targeting dihydrofolate reductase in Mycobacterium tuberculosis, J. Biol. Chem. 288 (2013) 23447–23456.